AFRL-OSR-VA-TR-2015-0210

Multidimensional Signal Processing for Sensing & Communications

Shannon Blunt
UNIVERSITY OF KANSAS CENTER FOR RESEARCH INC.

07/29/2015
Final Report

Air Force Research Laboratory
AF Office Of Scientific Research (AFOSR)/ RTC
Arlington, Virginia 22203
Air Force Materiel Command

REPORT DOCUMENTATION PAGE

Form Approved
OMB No. 0704-0188

1. REPORT DATE *(DD-MM-YYYY)*	2. REPORT TYPE	3. DATES COVERED *(From - To)*
03-08-2015	Final Performance	01-06-2012 to 31-05-2015

4. TITLE AND SUBTITLE
Multidimensional Signal Processing for Sensing & Communications

5a. CONTRACT NUMBER

5b. GRANT NUMBER
FA9550-12-1-0220

5c. PROGRAM ELEMENT NUMBER

6. AUTHOR(S)
Shannon Blunt

5d. PROJECT NUMBER

5e. TASK NUMBER

5f. WORK UNIT NUMBER

7. PERFORMING ORGANIZATION NAME(S) AND ADDRESS(ES)
UNIVERSITY OF KANSAS CENTER FOR RESEARCH INC.
2385 IRVING HILL RD
LAWRENCE, KS 660457563 US

8. PERFORMING ORGANIZATION REPORT NUMBER

9. SPONSORING/MONITORING AGENCY NAME(S) AND ADDRESS(ES)
AF Office of Scientific Research
875 N. Randolph St. Room 3112
Arlington, VA 22203

10. SPONSOR/MONITOR'S ACRONYM(S)
AFOSR

11. SPONSOR/MONITOR'S REPORT NUMBER(S)

12. DISTRIBUTION/AVAILABILITY STATEMENT
A DISTRIBUTION UNLIMITED: PB Public Release

13. SUPPLEMENTARY NOTES

14. ABSTRACT
The objective of this effort was to enhance sensitivity for radar and multi-mode communication systems in the presence of interference, which can be coupled across the dimensions of space, slow-time, and fast-time according to the operating mode. In particular, the effort focused on waveform-diverse emission schemes including MIMO radar, pulse-agile radar, and intra-pulse radar-embedded communications. Leveraging the notion of STAP used for clutter cancellation in airborne/space radar, the increase in degrees of freedom afforded by multidimensional coupling was explored to improve receive detection/estimation performance via the resulting increased diversity of the transmit signal. This effort addressed the mathematical modeling and optimization of multidimensional emissions through the use of analytical structures for physical waveform implementation. Likewise, appropriate structures for interference cancellation on receive were investigated. The waveform-diverse embedding of LPI communications into radar clutter was likewise examined.

15. SUBJECT TERMS
multidimensional signal processing

16. SECURITY CLASSIFICATION OF:			17. LIMITATION OF ABSTRACT	18. NUMBER OF PAGES	19a. NAME OF RESPONSIBLE PERSON
a. REPORT	b. ABSTRACT	c. THIS PAGE			Shannon Blunt
U	U	U	UU		19b. TELEPHONE NUMBER *(Include area code)* 785-864-7392

Standard Form 298 (Rev. 8/98)
Prescribed by ANSI Std. Z39.18

Final Report

Air Force Office of Scientific Research

Program Manager: Dr. Arje Nachman

Project Title: Multidimensional Signal Processing for Sensing & Communications

Award # FA9550-12-1-0220

Performance Period: 6/1/2012–5/31/2015

PI: Shannon D. Blunt

General Program Overview

The objective of this effort was to enhance sensitivity and develop new multi-mode formulations for radar and communications in the presence of interference, which may be coupled across the dimensions of space, slow-time, fast-time, and polarization according to the operating mode. In particular, the effort focused on waveform-diverse emission schemes such as various physically realizable forms of MIMO radar and polarization-diverse radar, adaptive receive processing for these waveform-diverse modes, and intra-pulse radar-embedded communications.

Leveraging the notion of STAP used for clutter cancellation in airborne/space radar, the multiplicative increase in degrees of freedom afforded by multidimensional coupling enables expansion to other dimensions as well. Performing this coupling on transmit also has the potential to improve receive detection/estimation performance via the resulting increased diversity of the transmit signal. This effort addressed the mathematical modeling and optimization of different multidimensional structures for the realization of new physical radar emissions which, when possible based on available test equipment, were also evaluated experimentally.

New adaptive receiver processing schemes were also likewise developed for these multidimensional emission structures which were also evaluated experimentally based on the availability of measurements. Finally, this effort continued the theoretical development of a scheme for waveform-diverse embedding of low probability of intercept communication symbols into radar clutter, along with associated symbol detection/decision processing, that was the focus of a previous AFOSR YIP award. It is expected that, upon transition, these waveform-diverse schemes will serve as enabling technology to support long-term Air Force initiatives to address an ever more congested and contested RF spectrum.

Section I: Multidimensional Physical Radar Emissions

As outlined in [1], which resulted from collaborative effort under the NATO SET-179 and SET-182 research task groups on "Dynamic Waveform Diversity & Design" and "Radar Spectrum Engineering & Management", respectively, there are multiple challenges facing the radar community as a result of an increasingly congested and contested RF spectrum. A promising approach to address these challenges is to leverage advances in waveform diversity [2] to determine how to better exploit the multiple dimensions in which a radar operates. This component of the project examined how to optimize physical radar emissions and then employed this same framework for the design of physical multidimensional emissions.

Optimization of Physical Waveforms

Within the context of the polyphase-coded FM (PCFM) framework [3,4], which established the means to convert arbitrary polyphase codes into physically realizable nonlinear FM (NLFM) waveforms amenable to the distortion induced by a radar transmitter, an optimization scheme was developed to search this very high dimensional space [5]. For a code with $N + 1$ chips, where each could take on one of M different values from a constant amplitude phase constellation, there are M^N possible nonlinear FM waveforms that could be generated for a given shaping filter $g(t)$ [4]. Clearly it is not possible to search this entire space if either M or N are moderately large (N closely approximately the waveform time-bandwidth product with practical values from roughly 50 up to several thousand). Since this large space precludes an exhaustive search for the global optimum, strategies are needed (e.g. [6,7]) to determine sufficiently good solutions according to the desired performance measure such as peak sidelobe level (PSL) or integrated sidelobe level (ISL).

Under this effort, a new search scheme was described in [5] that relies on the fact that PSL and ISL, along with a newly defined metric denoted as frequency template error (FTE) that relies on the Fourier relationship between autocorrelation and power spectral density [5], are all different measures of the waveform autocorrelation sidelobes. Using this relationship it is possible to employ a greedy search strategy that avoids the individual local minima of each metric by alternating between them. This strategy, denoted as "performance diversity" is a twist on multi-objective optimization in which, instead of seeking to balance between conflicting metrics, these complementary metrics provide different perspectives on the same underlying criterion: lower range sidelobes.

Using the benchmark of the PSL bound on hyperbolic FM (HFM) waveforms [8] defined as

$$\mathrm{PSL}_{\mathrm{HFM\,bound}} = -20\log_{10}(BT) - 3 \text{ dB}, \tag{1}$$

which is a function of time-bandwidth product (BT), it has been demonstrated that optimized PCFM waveforms can surpass this benchmark by a few dB for a given N (which well approximates BT). It will be demonstrated later that new ways to incorporate additional dimensionality into the waveform without increasing BT can go much further.

Figures 1 and 2 illustrates the sidelobes and mainlobe detail for use of the individual metrics (PSL, ISL, and FTE) and the performance diversity approach along with the LFM

waveform for comparison when $BT \cong N = 64$ and $M = 64$. In this case the PSL benchmark from (1) is found to be –39.1 dB. Table 1 provides a comparison of the three individual optimization metrics, performance diversity, and LFM in terms of PSL, ISL, and FTE as well as mainlobe resolution defined relative to the baseline LFM waveform. Note that, at a cost of only ~30% broadening of range resolution, the performance diversity optimized waveform surpasses the HFM bound by 1.1 dB (and it is the only waveform of this group to even get close to doing so).

In general we have observed that such optimized FM waveforms that can surpass the HFM bound largely retain the chirp-like structure of an LFM waveform due to the consolidation of much of the range-Doppler ambiguity into the well-known ridge that provides Doppler tolerance. Such waveforms exhibit the generic "sideways S" time-frequency shape that is typical of NLFM waveforms [8-12] (and summarized in [13]), albeit with seemingly random perturbations that arise from the optimization to break up the coherency that otherwise leads to higher range sidelobes. In fact, some of these optimized FM waveforms even contain short-term wideband components that are quite similar to aspects of calls generated by some species of bats [14], which unsurprisingly speaks to a degree of optimality in the bat call.

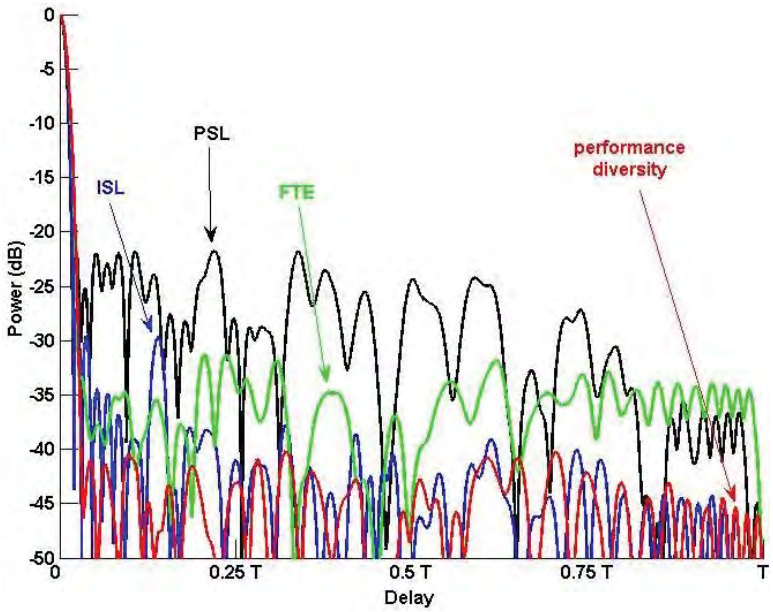

Figure 1: Autocorrelation of the optimized FM waveforms using the PSL, ISL, and FTE metrics individually and the performance diversity paradigm

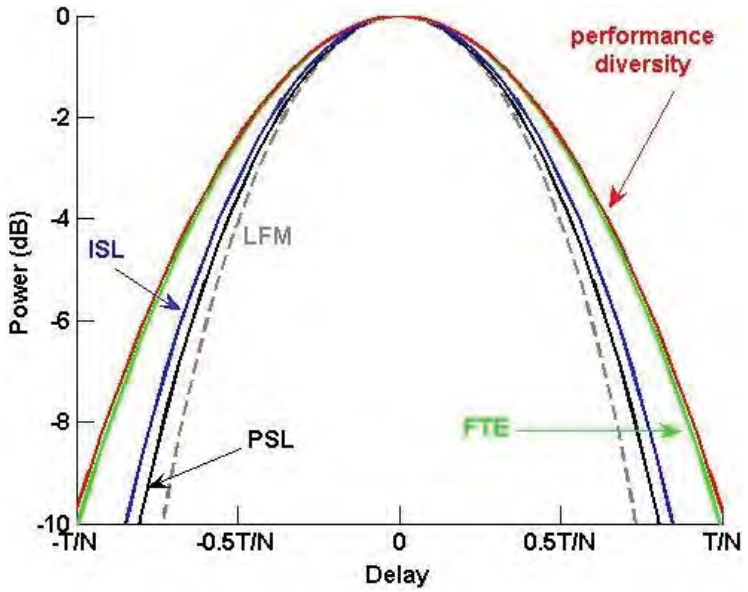

Figure 2: Autocorrelation of the optimized FM waveforms using the PSL, ISL, and FTE metrics individually and the performance diversity paradigm (mainlobe close-up)

Table 1: Quantified performance for optimized FM waveforms

		Optimization Metrics			
	LFM waveform	PSL only	ISL only	FTE only	Performance Diversity
final PSL value (dB)	−13.5	−21.1	−27.0	−31.3	−40.2
final ISL value (dB)	−9.8	−6.7	−20.0	−15.6	−24.9
final FTE value (dB)	−17.0	−16.6	−22.4	−30.1	−32.1
relative 3 dB resolution	1.00	1.06	1.11	1.26	1.28
relative 6 dB resolution	1.00	1.08	1.13	1.30	1.33

It is also described in [5] how, in addition to designing physical waveforms via optimization of the underlying coding of the PCFM framework, one may extend the optimization to encompass the impact of the distortion-inducing radar transmitter so as to ultimately optimize the physical emission that is launched into free space. Figure 3 depicts this arrangement in which the elements of the discrete code are collected into the vector **x**, the operation $T_{\text{PCFM}}\{\bullet\}$ converts the code **x** into a continuous PCFM waveform, and $T_{\text{Tx}}[\bullet]$ represents the distortion induced by the transmitter onto the waveform that subsequently produces the free-space emission. It is shown in [5] that both transmitter model-in-the-loop (MiLo) and hardware-in-the-loop (HiLo) optimization can be performed. The latter has thus far been demonstrated with low power systems using a Class A power amplifier (solid state). Future work will examine the impact of high power tube-based amplifiers (e.g. klystron) that are expected to induce greater distortion. Such an approach may provide significant benefit to ongoing work to better contain the spectral content of high-power radar emissions.

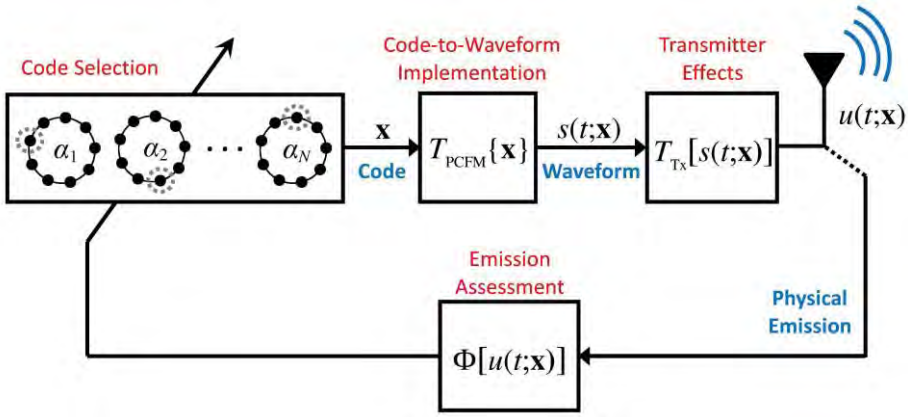

Figure 3: Mathematical representation for the optimization of PCFM radar emissions

Finally, leveraging previous work performed in collaboration with AFRL [15] involving the optimization of a non-repeating form of nonlinear FMCW waveform that is optimized on a segment-wise basis, the notion of time-hopping frequency gaps within a radar spectrum was explored [16]. Because it is essentially a form of FM noise radar, as long as the spectral gaps move sufficiently often the detrimental increase in sidelobes that would otherwise occur is largely avoided. Figure 4 illustrates the power spectral density for individual waveform segments within which fixed spectral gaps reside as well as the aggregated power spectral density in which these gaps are averaged out over time. The integrated autocorrelation over a coherent processing interval (Fig. 5) shows that moving the spectral gaps more often leads to better radar sensitivity. Future work will explore how this approach can facilitate the incorporation of frequency-hopped communications operating in tandem with the frequency-hopped radar spectral gaps.

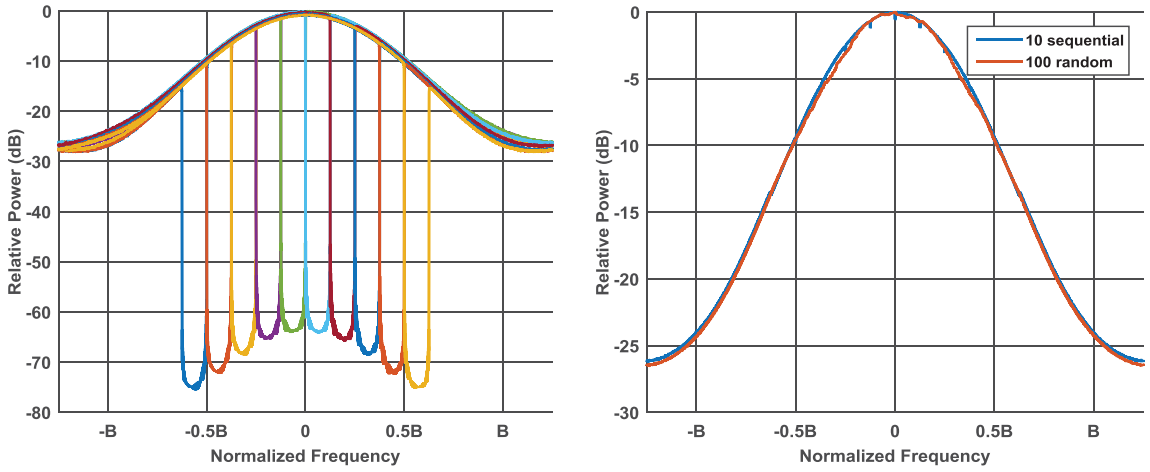

Figure 4: Power spectral density for (a) 10 sequentially hopped spectral gaps and (b) the aggregated power spectral density for the 10 sequentially hopped gaps and 100 randomly hopped gaps

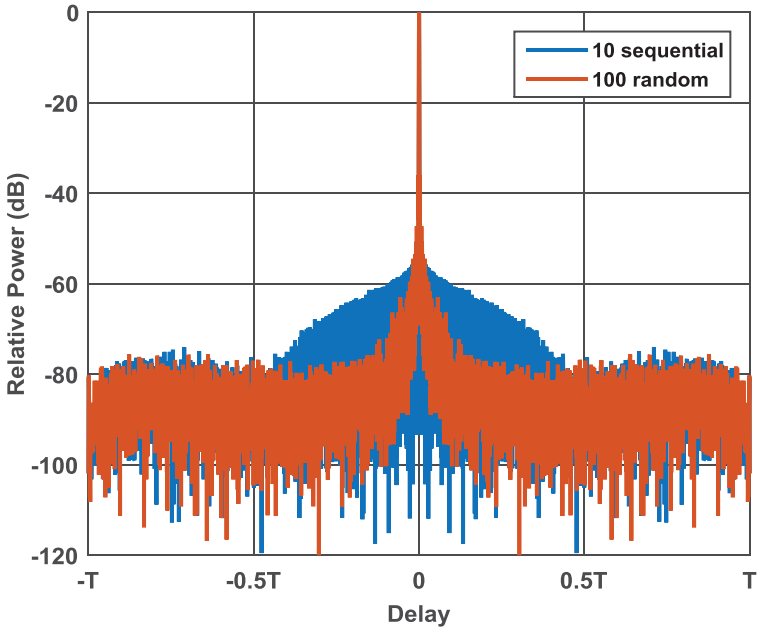

Figure 5: Integrated autocorrelation for the 10 sequential and 100 random hopped spectral gaps

Spatial Modulation of Physical Waveforms

The coded physical structure of the PCFM waveform makes it attractive as a framework from which to construct multidimensional emission schemes. One such scheme that was developed under this effort denoted as "spatial modulation" [17,18] incorporates an additional form of fast-time coding that is implemented in such a way as to control the spatial steering of the antenna array mainbeam during the pulse width. In so doing, the active radar illumination can mimic a similar passive attribute of the human eye (or any animal possessing fovea) known as *fixational eye movement* that has been found to enhance visual acuity and discrimination. Defined generally as the "waveform diverse array", this formulation also subsumes the notion of the frequency diverse array (e.g. [19-23]).

Defining $s(t\,;\mathbf{x})$ as the PCFM waveform generated by the underlying code $\mathbf{x}$, the actual waveform launched from the mth antenna element in a uniform linear array (ULA) can be expressed as

$$s_m(t,\theta_{\mathrm{C}};\mathbf{x},\mathbf{x}_{\mathrm{s}}) = \frac{1}{\sqrt{T}}\, s(t\,;\mathbf{x})\, b^m(t\,;\mathbf{x}_{\mathrm{s}})\,, \tag{2}$$

where

$$b(t\,;\mathbf{x}_{\mathrm{s}}) = \exp\left\{-j\left(\int_0^t g(\tau) * \left[\sum_{n=1}^{N} \varepsilon_n\, \delta\left(\tau-(n-1)T_p\right)\right] d\tau + \bar{\Delta}_0\right)\right\} \tag{3}$$

is the FM signal that steers the beam in fast time and $(\bullet)^m$ in (2) arises from the Vandermonde structure across the ULA. The vector $\mathbf{x}_s$ contains the sequence of electrical angle phase shifts $\varepsilon_1, \varepsilon_2, \ldots \varepsilon_N$ to steer the spatial beam in fast-time and $\bar{\Delta}_0$ is the initial electrical angle.

The far-field emission from an *M*-element antenna array that results from the combination of waveform and spatial modulation can be expressed as

$$g\left(t,\theta,\theta_C\right)=\frac{1}{M}\sum_{m=-(M-1)/2}^{(M-1)/2} s_m(t,\theta_C)\, e^{jm\,2\pi d\sin(\theta)/\lambda}\,, \tag{4}$$

for θ_C the center spatial direction of the beam (relative to boresight), d the antenna element spacing and λ the wavelength (assuming the narrowband assumption holds), with $\mathbf{x}$ and $\mathbf{x}_s$ omitted for compact representation. From (4) it can be observed that the waveform-modulated signal changes as a function of spatial angle, meaning that this formulation is a physically realizable form of MIMO radar. Further, by maintaining a coherent beam that is steered in fast-time, the spatially-modulated emission is less prone to degradation from array mutual coupling effects that can otherwise arise for arbitrary MIMO emissions [24,25] and that could potentially damage the radar [26,27] due to high voltage standing wave ratio (VSWR).

Using the emission structure of (4), the delay-angle dependent received signal that results from the reflection of the spatially modulated radar illumination is, for the *m*th antenna element,

$$y_m\left(t,\theta_C\right)=\int\left[x(t,\theta)*g(t,\theta,\theta_C)\, e^{jm\,2\pi d\sin(\theta)/\lambda}\right]d\theta+u(t)\,. \tag{5}$$

In (5), the term $x(t,\theta)$ is the complex scattering as a function of delay and spatial angle, $u(t)$ is additive noise, and $*$ represents convolution. Across the *M* antenna elements, the collection of the received signal defined by (5) provides a delay-angle coupled response from the illuminated environment, where the coupling naturally realizes a multiplicative increase in degrees of freedom for receive processing in the same manner as space-time adaptive processing (STAP) for airborne/space-based radar. The implications of delay-angle coupling for adaptive receive processing are demonstrated in Section II, where the non-uniform distribution of transmit energy as a function of spatial angle via $g\left(t,\theta,\theta_C\right)$ must be compensated so as not to induce a noise enhancement effect.

It is also instructive to examine the impact of this coupled emission when non-adaptive processing is performed that consists of standard beamforming and pulse compression (according to the waveform-modulated emission in each spatial direction). Figure 6 illustrates the non-adaptive processing responses when there are five targets in an 'X' formation in delay-angle for each of four different illumination schemes: Case 1) standard transmit beamforming (no spatial modulation), Case 2) a first null to first null linear spatial sweep, Case 3) a second null to second null linear spatial sweep, and Case

4) a first null to first null half-cycle sinusoidal spatial sweep. The waveform for all cases is an LFM with $BT \cong N = 200$ and the center direction is $\theta_C = 0°$ (boresight).

Because all but the center target reside near the mainbeam spatial nulls, the standard transmit beamforming (Case 1) only clearly identifies the center target. In contrast, the three spatial modulation illumination schemes provide much better visibility of all five targets, though with some reduced SNR that is due to spreading the transmit energy over a larger spatial angle and degraded range resolution due to less bandwidth being available for any given direction in the spatial sweep. It is clear that spatial modulation introduces a new tool for sensing in which SNR and range resolution can be traded for enhanced target visibility. Examination of the delay-angle ambiguity function [17,18] for these four emissions (Fig. 7) reveals that the three spatial modulation schemes also naturally provide enhanced spatial resolution as part of the trade. It is likewise interesting to note the impact of non-coherent combining of multiple pulses to exploit the phase diversity of different targets (Fig. 8), where the target configuration is now clearly visible for the three spatial modulation emission schemes.

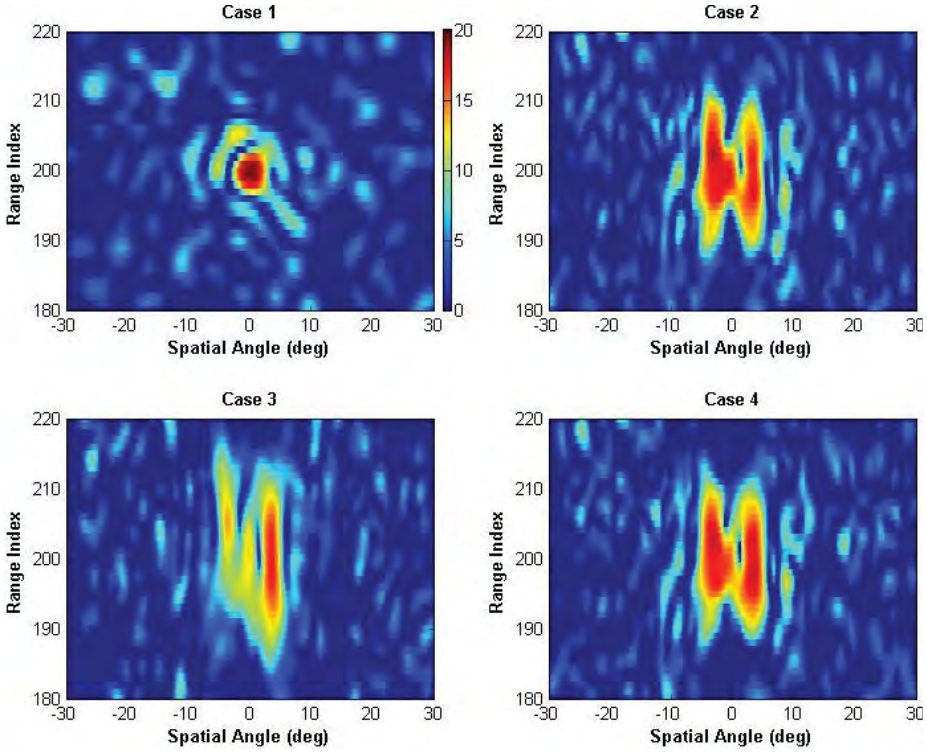

Figure 6: Five-target 'X' scenario for Case 1) standard beamforming, Case 2) null-to-null linear spatial modulation, Case 3) double null-to-null linear spatial modulation, Case 4) null-to-null half-cycle sinusoidal spatial modulation

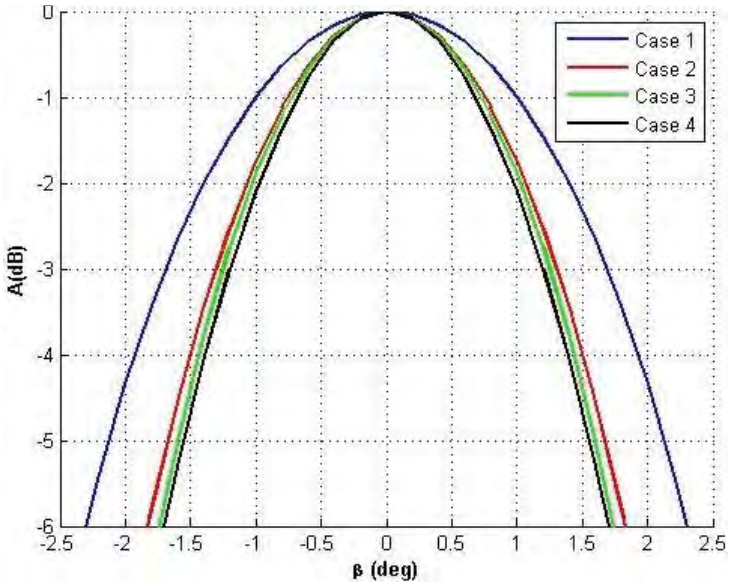

Figure 7: Peak-normalized $\tau = 0$, $\theta = 0°$ cut of angle-delay ambiguity function (mainbeam close-up) for Case 1) standard beamforming, Case 2) null-to-null linear spatial modulation, Case 3) double null-to-null linear spatial modulation, Case 4) null-to-null half-cycle sinusoidal spatial modulation

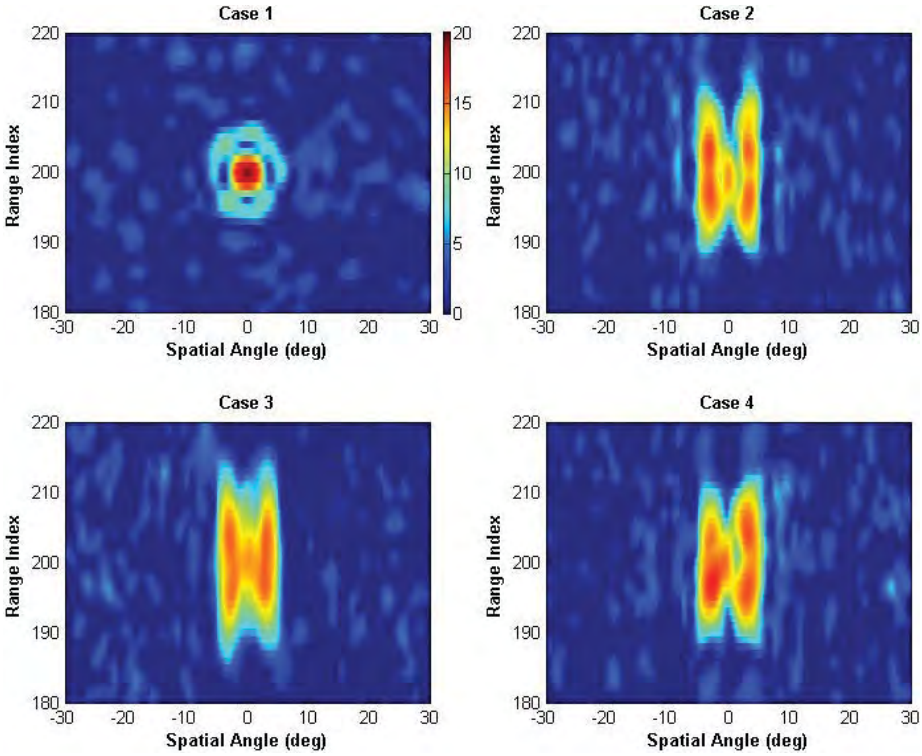

Figure 8: Four-pulse non-coherent integration of five-target 'X' scenario for Case 1) standard beamforming, Case 2) null-to-null linear spatial modulation, Case 3) double null-to-null linear spatial modulation, Case 4) null-to-null half-cycle sinusoidal spatial modulation

To better mimic the eye, a two-dimensional (2D) generalization of spatial modulation was demonstrated in [28] for a planar array. The spatially modulation FM signal from (3) now becomes

$$b_x(t;\mathbf{x}_{x,\mathrm{s}}) = \exp\left\{-j\left(\int_0^t g(\tau) * \left[\sum_{n=1}^{N} \varepsilon_{x,n}\,\delta\left(\tau-(n-1)T_p\right)\right] d\tau + \bar{\Delta}_{x,0}\right)\right\} \tag{6}$$

and

$$b_z(t;\mathbf{x}_{z,\mathrm{s}}) = \exp\left\{-j\left(\int_0^t g(\tau) * \left[\sum_{n=1}^{N} \varepsilon_{z,n}\,\delta\left(\tau-(n-1)T_p\right)\right] d\tau + \bar{\Delta}_{z,0}\right)\right\} \tag{7}$$

for x and z the azimuth and elevation designations, respectively. As a result, (2) generalizes to

$$s_{\mathbf{m}}(t,\theta_{x,\mathrm{c}},\theta_{z,\mathrm{c}};\mathbf{x}_{\mathrm{w}},\mathbf{x}_{x,\mathrm{s}},\mathbf{x}_{z,\mathrm{s}}) = \frac{1}{\sqrt{T}}\, s(t;\mathbf{x}_{\mathrm{w}}) \left(b_x(t;\mathbf{x}_{x,\mathrm{s}})\right)^{m_x} \left(b_z(t;\mathbf{x}_{z,\mathrm{s}})\right)^{m_z} \tag{8}$$

at the $\mathbf{m} = (m_x, m_z)$ antenna element so that the far-field emission is now

$$g\left(t,\theta_x,\theta_z\right) = \frac{1}{M_x M_z} \sum_{m_x}\sum_{m_z} s_{\mathbf{m}}(t) e^{j\left(k_x(\theta_x,\theta_z)m_x + k_z(\theta_z)m_z\right)}, \tag{9}$$

for k_x and k_z the associated wave numbers.

For comparison, consider the time-averaged beampatterns (over the pulse) shown in Fig. 9 that is comprised of standard beamforming, an optimized phase-dithered beamforming that is constant over the pulse, and spatial modulation that traces out one circular rotation during the pulse with a radius of the first null relative to the center direction. For two closely spaced targets residing at the same range, Fig. 10 illustrates the enhanced discrimination capability, where only the 2D spatial modulation can adequately discriminate the two targets from the sidelobes that are otherwise induced by either form of static beamforming. As with the 1D arrangement, SNR loss and range resolution degradation still occur with the 2D case. However, it is not difficult to imagine that, from a cognitive sensing standpoint, such trade-offs may be useful in some situations in much the same way that the eye performs autonomic adjustments based on lighting conditions and the degree of active attention [29-31].

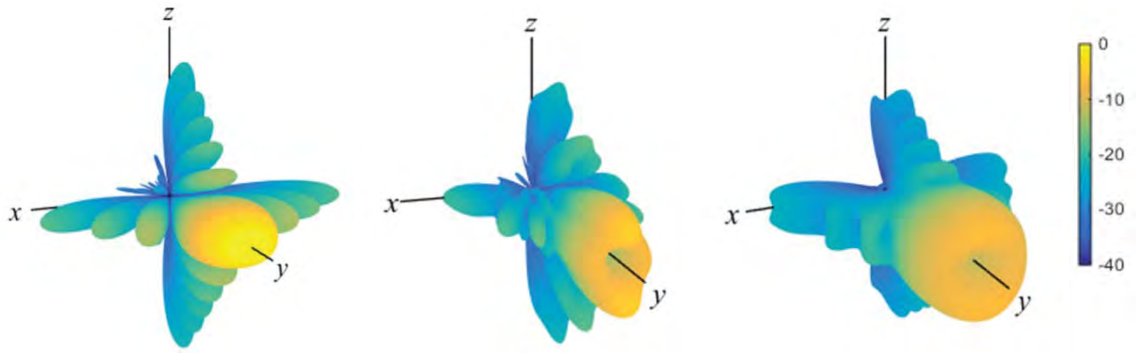

(a) (b) (c)

Figure 9: Aggregate beampattern in Cartesian coordinates for (a) standard beamforming; (b) phase-only beamforming; and (c) circular spatial modulation with center direction $(\theta_{x,c}, \theta_{z,c}) = (0°, 0°)$

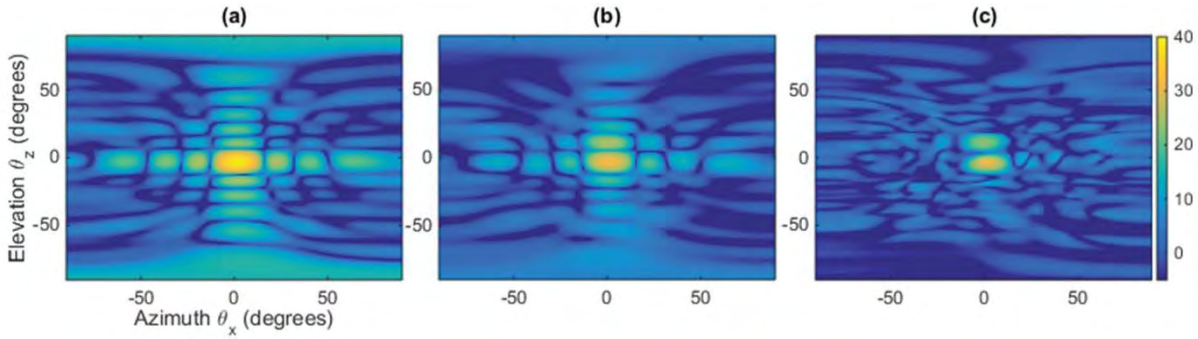

Figure 10: Received response for (a) standard beamforming (b) phase-only beamforming and (c) circular spatial modulation with targets located at $(0°, +11.5°)$ **and** $(+1.5°, -3°)$

Fast-Time Polarization Modulation

Along with the increased dimensionality of fast-time spatial modulation discussed above, this effort also explored the modulation of polarization in fast-time via a similar mechanism that is controlled by the waveform. In so doing, the waveform and polarization modulations are likewise coupled, thereby increasing the dimensionality of the radar emission, with applications such as weather radar [32] and polarimetric synthetic aperture radar (SAR) [33].

The simplest way in which fast-time polarization modulation can be achieved is well-known as it simply involves simultaneously emitting a different waveform on the horizontal and vertical elements of a dual-polarized antenna [34,35]. Since the desire is often to separate the co-polarized and cross-polarized components of the received signals on the horizontal and vertical elements, these waveforms should have low cross-correlation, with the most common waveforms meeting this criterion being an LFM up-chirp and down-chirp. In this case the instantaneous polarization during the pulse will lie somewhere on the great circle shown on the Poincaré sphere in Fig. 11.

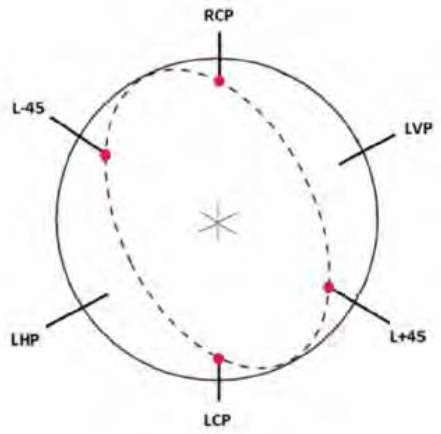

Figure 11: Feasible polarizations on the Poincaré sphere for two waveforms directly connected to horizontal and vertical antenna elements. RCP: right-hand circular, LCP: left-hand circular, LHP: linear horizontal, LVP: linear vertical, L-45: linear with –45° tilt, L+45: linear with +45° tilt

We have recently shown that the PCFM waveform structure can be combined with a 180° hybrid coupler to achieve linear amplification using nonlinear components (LINC) out of the sum channel of the hybrid as a means to slow down the rapid pulse rise/fall-time that dominates the spectral roll-off of the radar emission [36]. In this case an additional form of coding is introduced that is used to control the relative phase between two otherwise identical waveforms such that, when the two waveforms are combined in phase within the hybrid the amplitude can be controlled (in this case after the high power amplifier that is operated in saturation).

This same idea was subsequently applied to polarization modulation (Fig. 12), where Σ is the sum channel, Δ is the difference channel, and κ is an additional phase term that dictates the particular great circle that can be traversed on the Poincaré sphere. The waveforms $s_1(t)$ and $s_2(t)$ are coded such that, when combined in the hybrid, they produce the resulting $s_H(t)$ and $s_V(t)$ waveforms that are emitted from the horizontal and vertical antenna elements, respectively, to produce the desired joint waveform/polarization modulation [37,38].

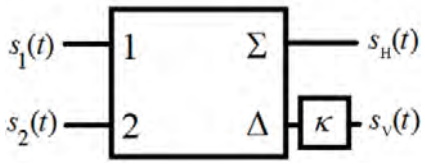

Figure 12: 180° hybrid for polarization control

Mathematically, the result from the hybrid is

$$s_H(t) = \frac{1}{\sqrt{2}}(s_1(t) + s_2(t)) \tag{10}$$

$$s_V(t) = \frac{1}{\sqrt{2}}(s_2(t) - s_1(t))\exp(j\kappa)\,. \tag{11}$$

For the examples of κ = 0° and κ = –90°, the associated great circles on the Poincaré sphere are shown in Fig. 13. Via control of the two driving waveforms and phase term κ any polarization state on the surface of the Poincaré sphere can be attained.

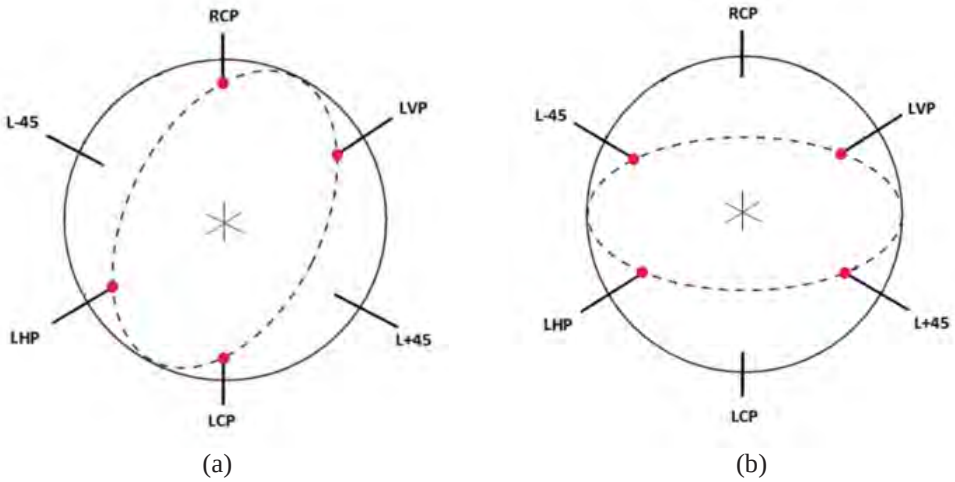

(a) (b)

Figure 13: Feasible polarizations on the Poincaré sphere using the 180° hybrid for a) κ = 0°, and b) κ = –90°. RCP: right-hand circular, LCP: left-hand circular, LHP: linear horizontal, LVP: linear vertical, L-45: linear with –45° tilt, L+45: linear with +45° tilt

The waveforms above can be coded to enable control over the joint waveform/polarization modulation by again leveraging the PCFM structure as

$$s_1(t) = \exp\left\{ j\left(\int_0^t g(\tau) * \left[\sum_{n=1}^{N} (\alpha_n + \beta_n)\delta\left(\tau - (n-1)T_p\right) \right] d\tau + \phi_0 + \psi_0 \right) \right\} \tag{12}$$

$$s_2(t) = \exp\left\{ j\left(\int_0^t g(\tau) * \left[\sum_{n=1}^{N} (\alpha_n - \beta_n)\delta\left(\tau - (n-1)T_p\right) \right] d\tau + \phi_0 - \psi_0 \right) \right\} \tag{13}$$

where α_n is the original PCFM waveform coding, β_n serves as a fast-time polarization coding about the particular great circle of the Poincaré sphere determined by the value of κ, and ϕ_0 and ψ_0 dictate the initial waveform phase and polarization state, respectively. This formulation will be continued to be explored to determine the utility of joint waveform/polarization modulation with regard to various sensing applications, metrics by which this emission scheme may best be evaluated and optimized, and for broader

applicability such as to encode communications into polarization state. In Section II a new adaptive processing scheme is described that is applicable to dual-polarized emissions.

Expanding Waveform Degrees of Freedom beyond the Time-Bandwidth Product

The time-bandwidth product (*BT*) of a waveform is a measure of the dimensionality of the waveform. As defined in (1), the peak sidelobe level (PSL) for the HFM waveform has a known bound that serves as a benchmark for other FM waveforms. In this context the time aspect corresponds to the pulsewidth and the bandwidth corresponds to the 3 dB bandwidth (which is associated with matched filter range resolution). This component of the project focused on how to enhance waveform sensitivity (reduce sidelobes) further beyond the HFM bound while maintaining the same *BT*.

The PCFM waveform structure described above enables conversion of an arbitrary polyphase code into an FM waveform. The constellation of phase values from which a code can be drawn resides on the unit circle, where PCFM converts the phase change between successive code values into a continuous phase signal. The notion of "over-coding" described in [39,40] expands this arrangement to permit 1) freedom for additional phase trajectory changes during a chip interval and 2) a greater amount of phase change during a fixed interval as long as the aggregate power spectral density of the waveform does not exceed a specified spectral mask. The former enables even finer "phase dithering" during the pulse, an attribute that has been observed to reduce sidelobes by breaking up their coherence. The latter enables the instantaneous frequency content of the waveform to increase as long as it occurs rarely and thus conforms to the desired power spectral density.

Figure 14 illustrates the autocorrelation of three optimized PCFM waveforms, two of which employ over-coding. The variable L defines the number of phase "sub-transitions" during a chip width and M defines the amount of phase transition allowed during a chip width ($\pm M\pi$ so $M > 1$ exceeds the previous polyphase-code-based structure defined on the unit circle). Compared to a PSL of –41.4 dB without over-coding (L=1, M=1), which itself surpasses the HFM PSL bound of –39.1 dB by 2.3 dB, the (L=8, M=1) and (L=8, M=2) over-coded waveforms achieve PSL values of –44.1 dB and –52.0 dB, respectively, with the latter necessitating a spectral mask to prevent the 3 dB bandwidth from increasing. The sensitivity enhancement arises from increased design degrees of freedom that are evident from the now more rapid variation of instantaneous frequency (see Fig. 15).

The power spectral density is shown in Fig. 16 (with the (L=8, M=1) case replaced by an optimized (L=4, M=2) case to show a different combination of parameters). In particular, note that the M = 2 cases exhibit some spectral spreading (or "spectral fuzz") in the roll-off region, though the imposed Gaussian power spectral density mask is still maintained. Thus this notion of over-coding raises the fundamental question of, for a prescribed spectral mask that dictates roll-off and mainlobe width (to define range resolution), just how low can the range sidelobes be driven for a constant amplitude waveform? Note that our group recently showed [41] that a small amount of amplitude modulation (with associated mismatch loss of ~0.25 dB) can, if jointly optimized with the

FM waveform, achieve a physical emission with sidelobes below –108 dB in simulation and –83 dB demonstrated experimentally.

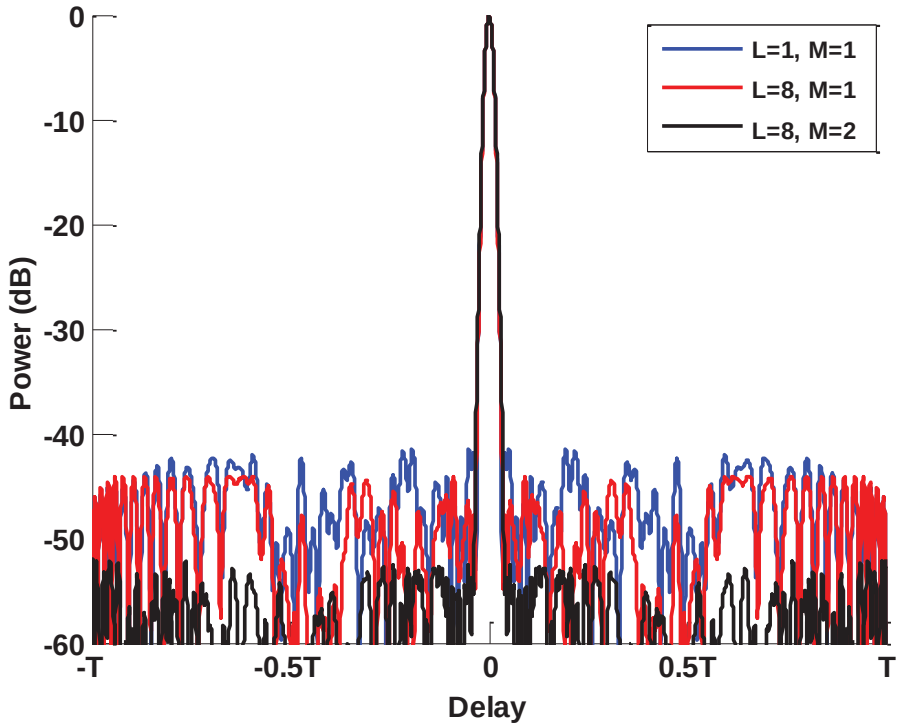

Figure 14: Autocorrelation comparison for over-coded optimized waveforms (*L*=8, *M*=1 and *L*=8, *M*=2) relative to the non-over-coded optimized waveform (*L*=1, *M*=1) for *BT* ≅ 64

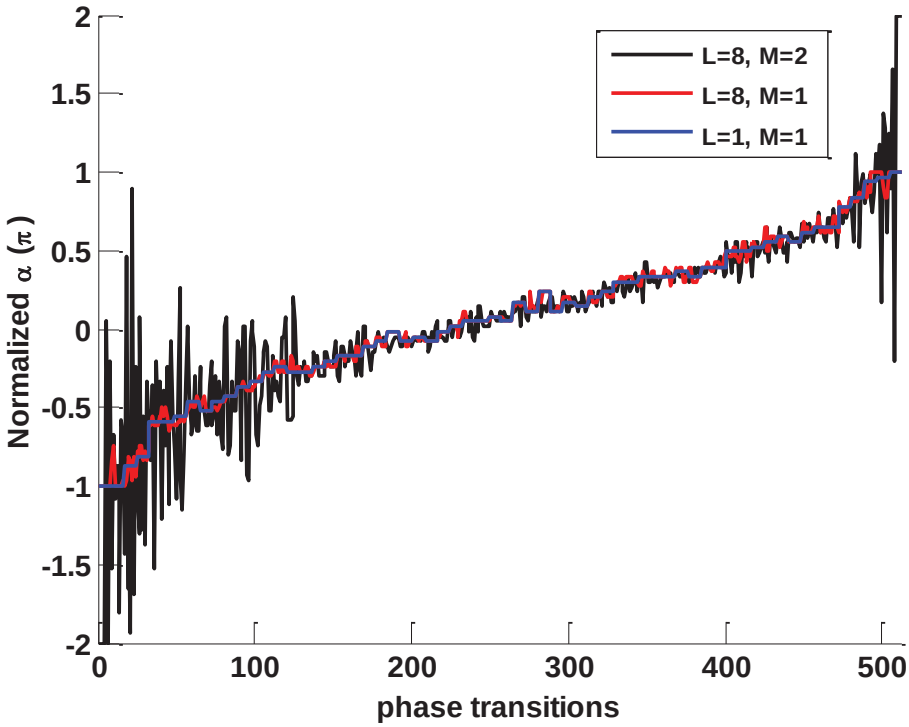

Figure 15: Normalized instantaneous frequency for the three waveforms

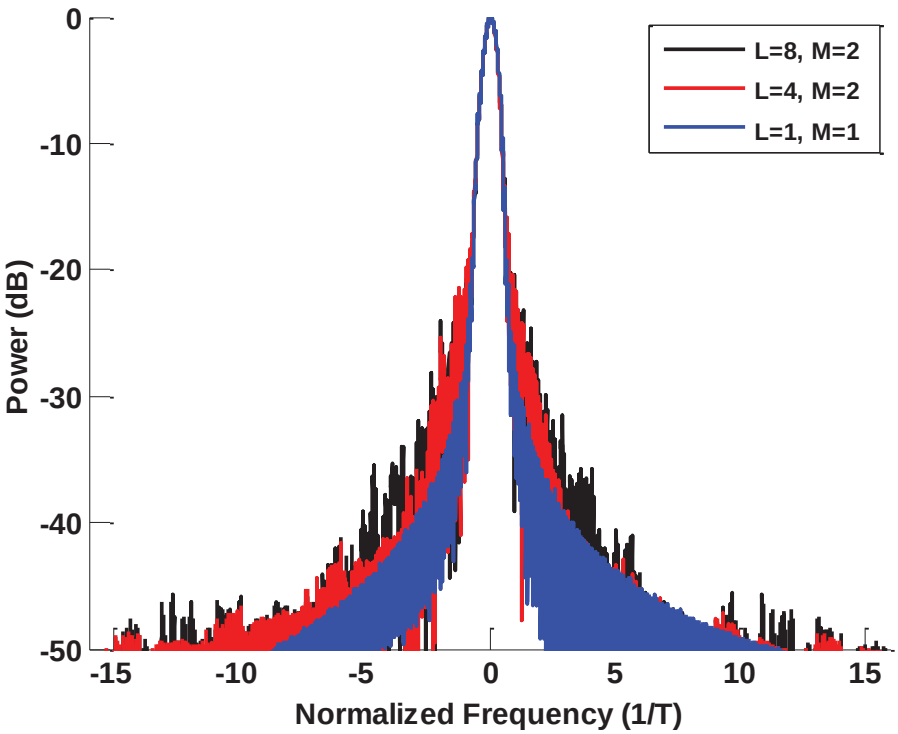

Figure 16: Power spectral density for over-coded waveforms - note the (*L* = 4, *M* = 2) waveform has replaced the (*L* = 8, *M* = 1) waveform here to show a different combination

Alternative to over-coding, in [42,43] a higher-order framework for PCFM waveforms was described. Defining the instantaneous waveform phase as $\phi(t)$, a combined first, second, and third order phase formulation can be expressed as

$$\phi_3(t) = \int_0^t \int_0^\tau \int_0^{\tau'} c(\tau'')\, d\tau''\, d\tau'\, d\tau + \int_0^t \int_0^\tau b(\tau')\, d\tau'\, d\tau + \int_0^t a(\tau)\, d\tau + \phi_{3,0} \tag{14}$$

where

$$a(\tau) = \sum_{n=1}^{N} \alpha_n\, g_1\left(\tau - (n-1)T_p\right) \tag{15}$$

is the first-order coded function according to the values in the sequence α_n and initial phase $\phi_{3,0}$, which collectively represent the original PCFM framework. The term

$$b(\tau') = \sum_{n=1}^{N} b_n\, g_2\left(\tau' - (n-1)T_p\right) \tag{16}$$

is the second-order coded function representing time-varying chirp-rate according to the values in the sequence b_n while

$$c(\tau") = \sum_{n=1}^{N} c_n \, g_3\left(\tau" - (n-1)T_p\right) \tag{17}$$

is the third-order coded function representing time-varying *chirp acceleration* according to the values in the sequence c_n. The terms $g_1(\tau)$, $g_2(\tau')$, and $g_3(\tau")$ are the associated shaping filters for each order. Thus (14) involves three different coding structures that can be manipulated to define a given FM waveform. It has been found that the first and second order terms yield the greatest benefit to designing good radar waveforms. A smaller additional benefit is obtained from the third order term with improvement continuing to diminish rapidly as the order increases further. For example, Fig. 17 depicts the autocorrelations of waveforms that were jointly optimized across the different orders. When the 2nd and 1st orders were jointly optimized a PSL value of –48.4 dB was attained. When the 3rd order component was incorporated for joint optimization the PSL only improved to –48.7 dB (a difference of 0.3 dB).

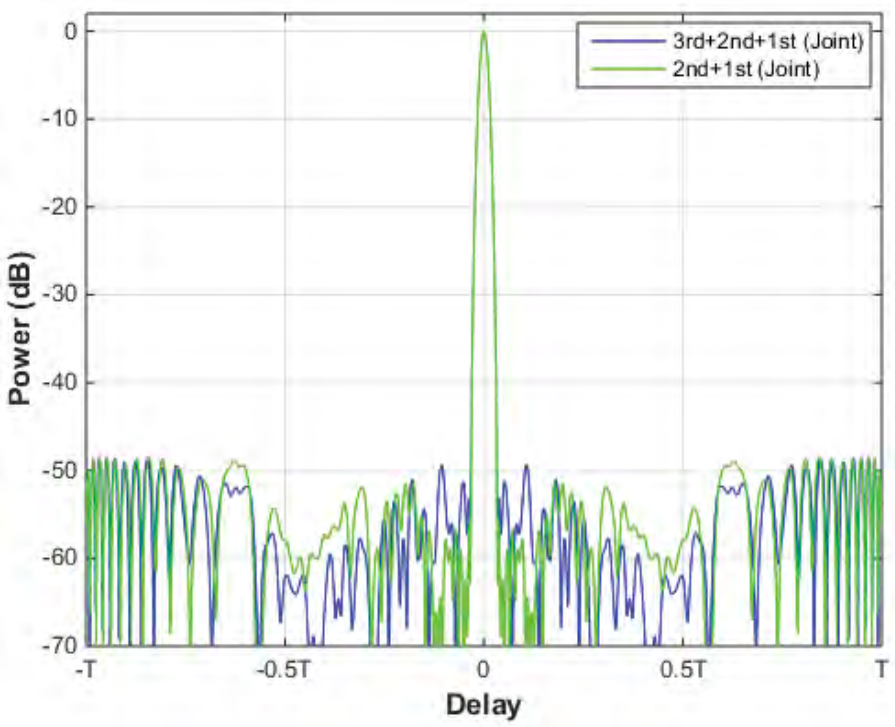

Figure 17: Autocorrelations of jointly optimized waveforms

It is interesting to consider the instantaneous frequency for these two waveforms as shown in Fig. 18. The familiar NLFM structure is apparent, though a close examination reveals the small dithering that is typical of PCFM to break up sidelobe coherence. Future

work will investigate the combination of this higher-order framework with the above over-coding scheme.

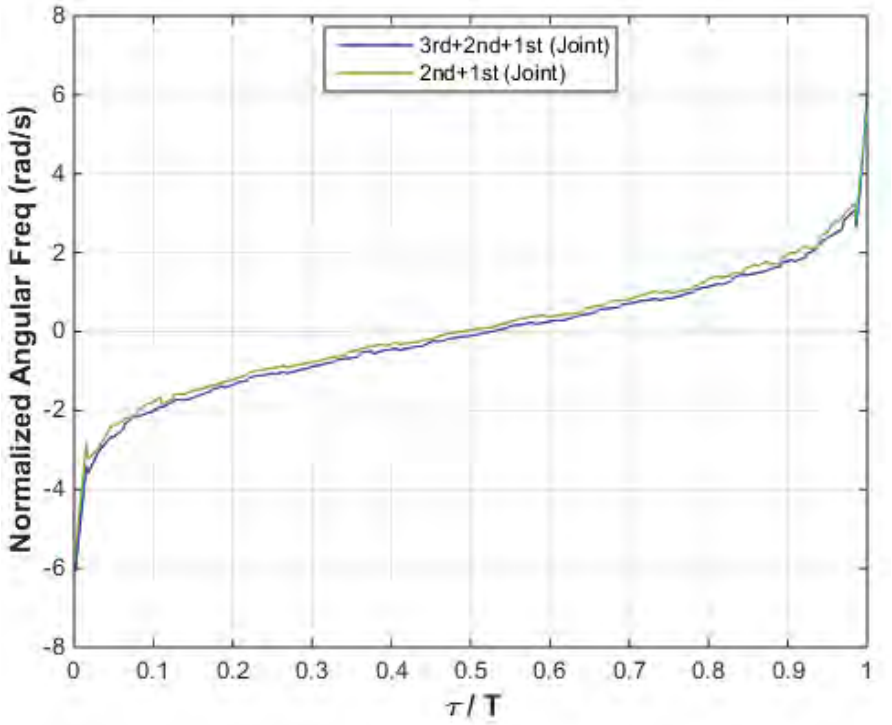

Figure 18: Instantaneous frequency of jointly optimized waveforms

Section II: Multidimensional Adaptive Receive Processing

In Section I multiple new physical emission schemes were described. While the straightforward matched filter may be applied to the resulting received echoes, it is useful for many applications to perform some form of optimal or adaptive receive processing. However, previous methods for optimal [44] and adaptive pulse compression [45] were based on a (non-physical) polyphase code framework that is not directly extensible to physical waveforms.

This component of the project focused on the generalization of the adaptive pulse compression (APC) algorithm to permit application to FM waveforms which constitute the majority of high-power radar emissions being used in practice. The framework of the problem can be stated as follows:

1. The phase function for an FM waveform is continuously changing and thus the waveform must be sampled at a rate high enough to provide acceptable fidelity (greater than the 3 dB bandwidth to account for sufficient spectral roll-off since a time-limited pulse has theoretically infinite bandwidth).
2. Such "over-sampling" with respect to 3 dB bandwidth results in higher dimensionality that
    a. increases computational cost,
    b. leads to ill-conditioning effects when sidelobes are suppressed (for optimal and adaptive processing),
    c. induces a range super-resolution condition that produces spurious sidelobe peaks.
3. Addressing the above issues then enables application of adaptive processing to physical emissions that possess spatial diversity, polarization diversity, etc. via incorporation/compensation of the salient physical features.

In [46,47] the APC structure has been generalized to account for these physical effects through the combination of 1) an MVDR-based structure to prevent over-nulling [48], 2) a polyphase decomposed representation of multiple delay-shifted versions of the over-sampled waveform [49], and 3) a "beam spoiling" modification to prevent the degradation associated with super-resolution [50] (relative to the matched filter). Figure 19 shows experimentally measured results using an LFM waveform taken from the roof of Nichols Hall on the University of Kansas campus. These receive-processed results include the new version of APC along with the traditional matched filter (MF) and two new instantiations of Least-Squares optimal mismatch filtering (MMF) suited to FM waveforms. The MMF results clearly outperform the MF, though the APC results yield the most significant enhancement. Using an optimized FM waveform from Section I reveals similar performance (Fig. 20), though the difference between the different receive processing schemes is less significant due to use of a far better waveform.

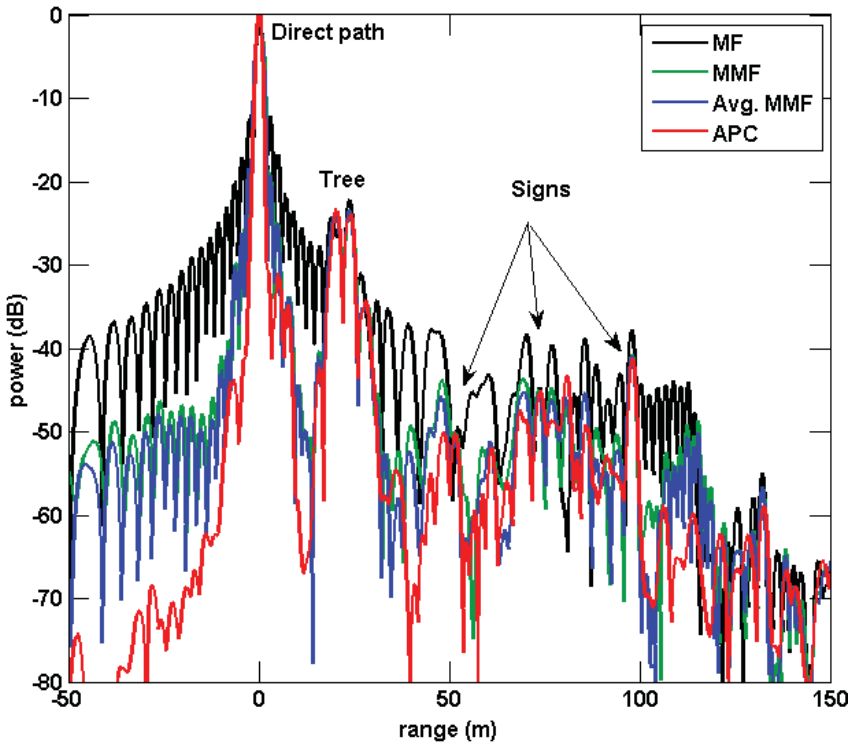

Figure 19: Pulse compressed response using LFM waveform (simultaneous transmit and receive using separate antennas so direct path dominates)

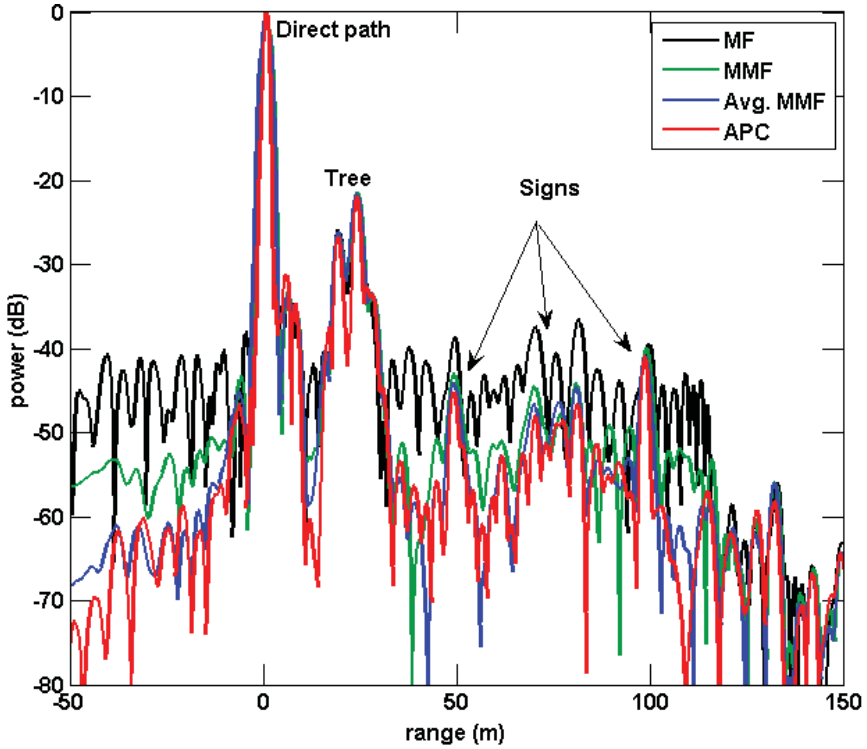

Figure 20: Pulse compressed response using optimized FM waveform (simultaneous transmit and receive using separate antennas so direct path dominates)

The version of APC amenable to physical FM waveforms has also been extended to incorporate physical MIMO emissions. Subsuming previous work on direction of arrival estimation [51,52] and a prior instantiation developed for (non-physical) polyphase codes [53], this approach is denoted as space-range adaptive processing (SRAP) as it jointly operates in the range and spatial angle domains [54]. For the spatial modulation scheme described in Section I, Fig. 21 depicts the matched filter and SRAP responses, respectively, when five proximate targets are illuminated by a spatially modulated emission that linearly sweeps in both frequency and angle. It is observed that SRAP suppresses delay-angle sidelobes and enhances resolution in both the range and spatial domains. This enhanced discrimination capability tends to incur a cost in terms of SNR so such an approach is likely to be most applicable when SNR is sufficiently high to permit enhanced discrimination. The mathematical derivation and implementation of SRAP can be found in [54].

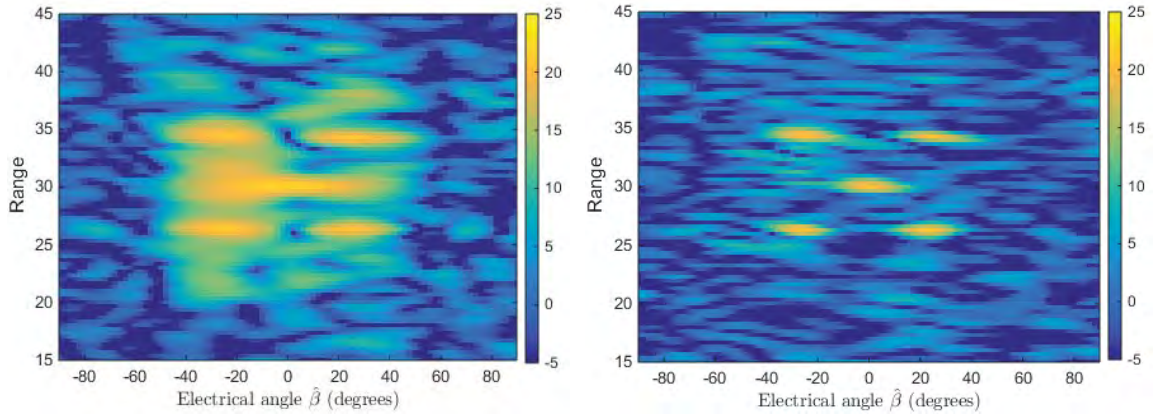

(a) (b)

Figure 21: Five targets illuminated by spatially modulated emission using (a) delay-angle matched filtering and (b) the SRAP algorithm

This waveform-based adaptive framework has also been developed for application to simultaneous dual-polarized radar emissions as a means to disambiguate the co-polarized and cross-polarized reflections at the radar receiver. The polarimetric APC (PAPC) algorithm derived in [37,38] realizes a different adaptive range-domain filter for each individual range cell and received polarization state. An experimental demonstration of this capability is illustrated in Fig. 22. An up-chirp and down-chirp having $BT = 100$ were concurrently emitted from the horizontal and vertical polarized elements using a dual-pol Vivaldi antenna. An identical antenna was used on receive to enable simultaneous transmit and receive. As with the above results, the direct path becomes the dominant signal that masks many of the smaller proximate echoes. A dihedral corner reflector was present about 97 m from the radar testbed which shows up clearly in the cross-polarized responses.

The blue trace in the data is the matched filter response that demonstrates the usual cross-correlation one expects from using two waveforms and which masks the smaller scatterers. The ultra-low sidelobe (ULS) response [41] (green trace) is obtained from using an optimized waveform that is emitted from the H and V antennas at separate times

to obtain an estimate of ground truth. We find that the PAPC algorithm operating on the echoes from the up/down-chirp waveforms (red trace) exhibits performance that is nearly identical to the time-separated optimized ULS response (e.g. the small echo from Nichols Hall is now observable). Thus one can conclude that PAPC provides an adaptive solution to enable simultaneous dual-polarized radar emissions.

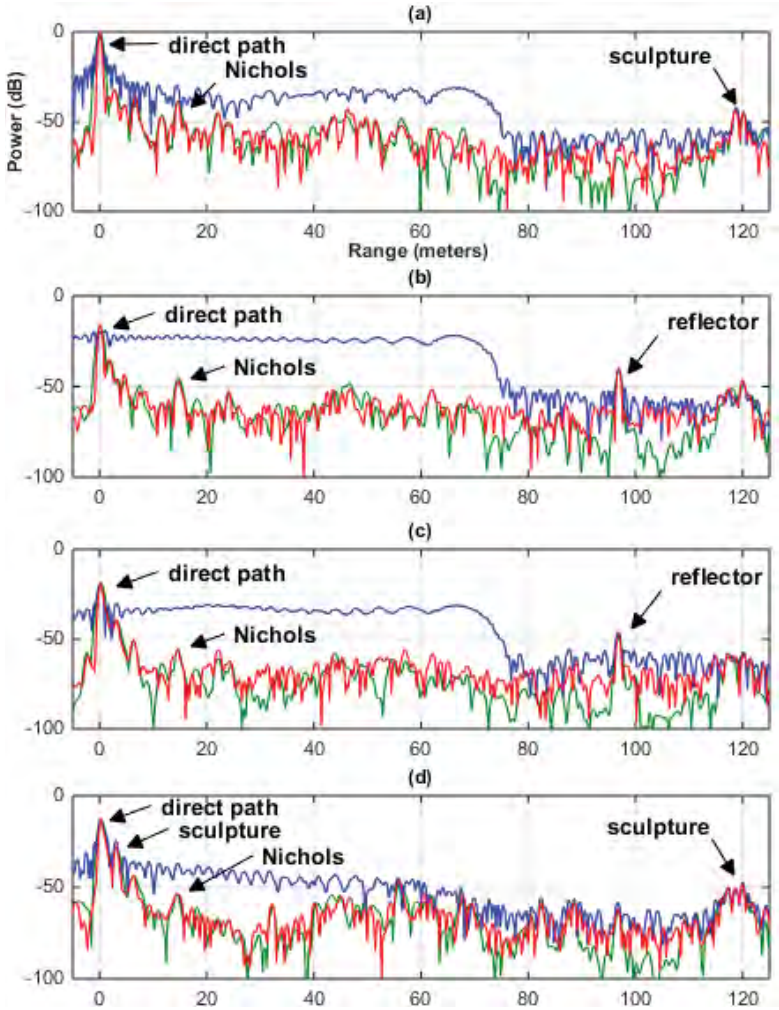

Figure 22: Experimental demonstration of adaptive separation of radar echoes generated by simultaneous dual-polarized radar emissions. (a) HH response; (b) HV response; (c)VH response; (d) VV response. Matched Filter (blue), PAPC (red) and ULS (green).

Section III: Intra-Pulse Radar-Embedded Communications

This final aspect of the project continued the investigation of a form of covert communication embedded via a tag/transponder into radar backscatter (i.e. clutter) that was the main focus of a previous AFOSR YIP project [55-57]. Recently in [58] the practical aspects of this problem were delineated to provide a framework for continued development, both theoretical and experimental (see Table 2).

Table 2: Practical design constraints for intra-pulse radar-embedded communications

1. Radar, tag, and desired receiver are not synchronized (no control channel available).
2. Communication symbols must be determined independently at the tag and desired receiver based on the observed radar illumination (must address possible timing uncertainty and multipath differences).
3. The surrounding clutter structure within which the symbols are to be covertly embedded is not known exactly, though the clutter response can be viewed as a random signal convolved with the radar waveform.
4. Symbols should be designed to be partially correlated with the clutter response (in the range domain) but still separable from one another on receive.
5. Symbols should have a temporal and spectral footprint commensurate with the radar waveform to ensure proper masking by the clutter and thus remain low probability of intercept (LPI).
6. Symbol design must occur in a reasonable time frame (while radar illumination persists).

It is analytically demonstrated in [58] that spectral shaping of the set of communication symbols (Fig. 23) according to the spectral footprint of the radar emission (and thus resulting clutter response) enhances the desired low intercept probability (LPI) attribute of the symbols while retaining good communication performance in terms of bit error rate. Specifically, the processing gain at a desired receiver that has knowledge of the possible symbols is evaluated for different symbol design strategies (Fig. 24). These same symbol strategies were likewise evaluated according to the processing gain that would be obtained at a hypothetical "worst case" intercept receiver that possesses partial clairvoyant knowledge of the symbols (i.e. their time width and bandwidth).

The comparison of these two processing gains then reveals the *gain advantage* of the desired receiver thereby realizing the underlying design metric that captures the fundamental goodness of a given symbol design approach (e.g. Fig. 25). Of the various symbol design strategies considered, it was the Shaped Water Filling (SWF) approach that was found to provide the best all-around performance in terms of minimizing communication error rate and ensuring LPI [58].

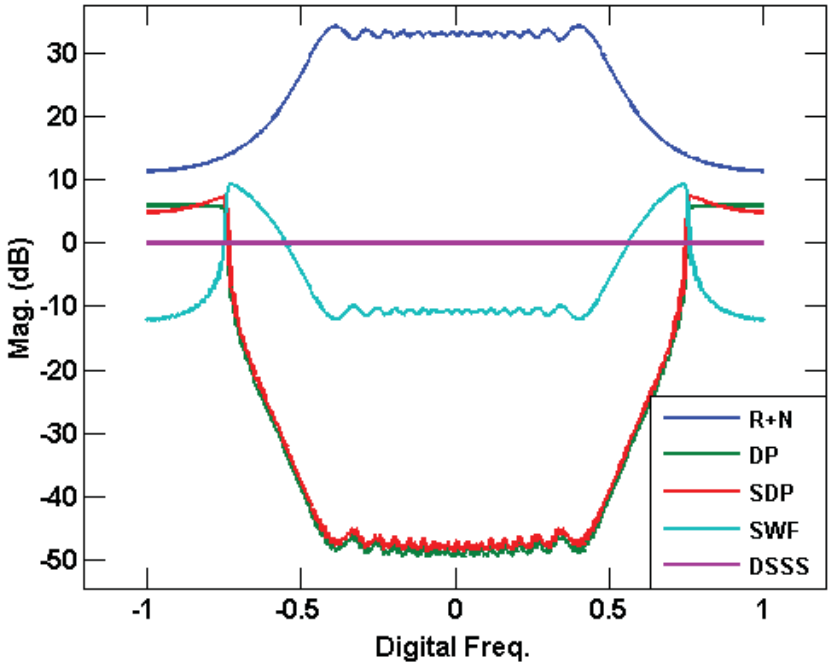

Figure 23: Spectral content for radar-embedded communication symbols where R+N: radar emission with noise, DP: dominant projection symbols, SDP: shaped dominant projection symbols, SWF: shaped water filling symbols, and DSSS: direct-sequence spread spectrum symbols (for baseline comparison).

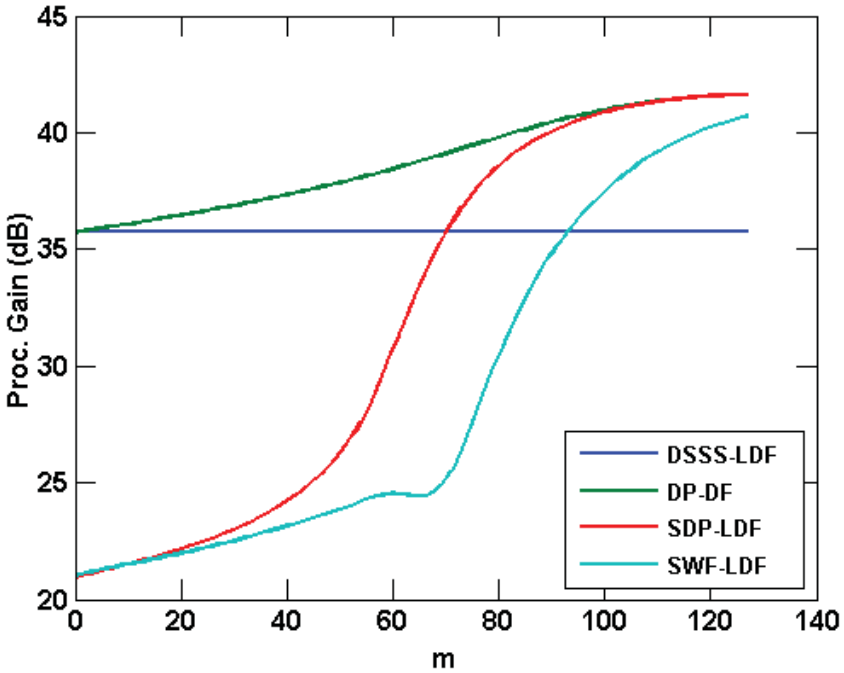

Figure 24: Comparison of processing gain as a function of symbol dimensionality *m* for 30 dB radar clutter to noise ratio using "best" observed receiver filtering (DF: decorrelating filter or LDF: loaded decorrelating filter) for each symbol set.

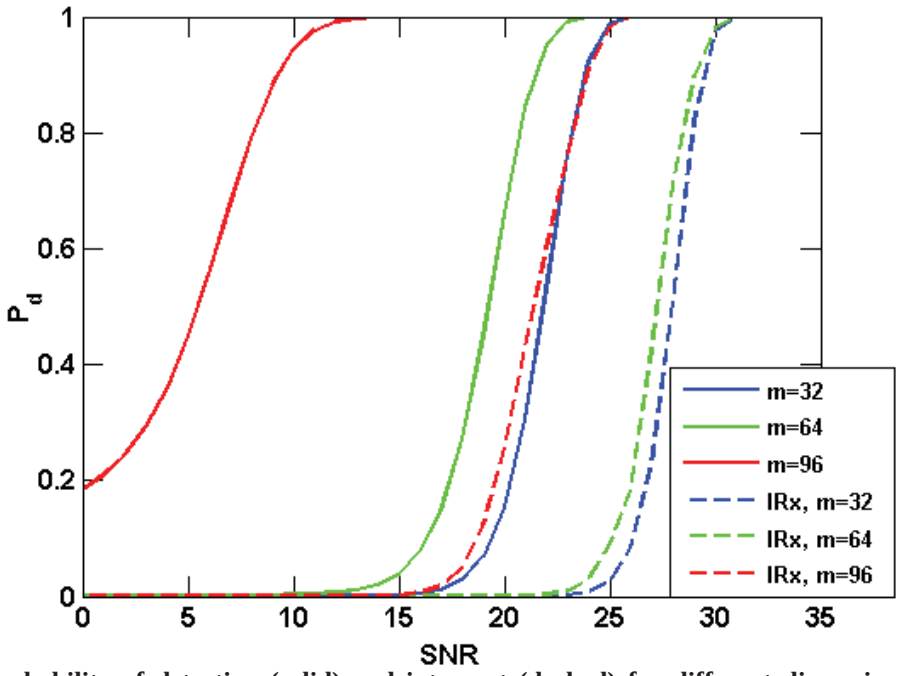

Figure 25: Probability of detection (solid) and intercept (dashed) for different dimensionalities of SWF symbols. The SNR difference for the same dimensionality demonstrates the gain advantage.

Publications

NATO Reports

1. S.D. Blunt, L. Savy, R. Adve, L. Cohen, U. Doyuran, G. Fabrizio, H. Griffiths, J.-P. Guyvarch, T. Higgins, S. Kemkemian, J. Klare, E. Mokole, S. Seguin, P. Serafin, A. Shackelford, R.F. Tigrek, and T. Webster, *Dynamic Waveform Diversity and Design*, Final Report of Task Group NATO SET-179, in release review, 2015.
2. H. Griffiths, L. Cohen, C. Baylis, S.D. Blunt, O. Forgeot, T. Higgins, E. Mokole, M. Nouvel, S. Seguin, N. Sentenac, A. Shackelford, R.F. Tigrek, *Radar Spectrum Engineering and Management*, Final Report of Task Group NATO SET-182, in release review, 2015.

Book Chapters

1. Chapter 46, "Radar Waveforms: Advanced Concepts," S.D. Blunt, in *Stimson's Introduction to Airborne Radar, 3rd edition*, H. Griffiths and C. Baker, eds., SciTech-IET, 2014.
2. S.D. Blunt, J. Jakabosky, and C. Allen, "Holistic Design of Physical Radar Emissions," in preparation for *Novel Radar Techniques & Applications*, R. Klemm, ed., *IET*, 2016.

Journal

1. S.D. Blunt, J. Jakabosky, M. Cook, J. Stiles, S. Seguin, and E.L. Mokole, "Polyphase-Coded FM (PCFM) Radar Waveforms, Part II: Optimization," *IEEE Trans. Aerospace & Electronic Systems*, vol. 50, no. 3, pp. 2230-2241, July 2014.
2. S.D. Blunt, P. McCormick, T. Higgins, and M. Rangaswamy, "Physical Emission of Spatially-Modulated Radar," *IET Radar, Sonar & Navigation*, vol. 8, no. 12, pp. 1234-1246, Dec. 2014.
3. P. McCormick, T. Higgins, S.D. Blunt, and M. Rangaswamy, "Adaptive Receive Processing of Spatially-Modulated Physical Radar Emissions," accepted to *IEEE Journal of Special Topics in Signal Processing*. (special issue on Advanced Signal Processing Techniques for Radar Applications)
4. J.G. Metcalf, C. Sahin, S.D. Blunt, and M. Rangaswamy, "Analysis of Symbol Design Strategies for Intrapulse Radar-Embedded Communications," accepted to *IEEE Trans. Aerospace & Electronic Systems*.
5. P. McCormick, J. Jakabosky, S.D. Blunt, C. Allen, and B. Himed, "Adaptive Polarimetric Radar Receive Processing and Fast-Time Polarization Modulation," in preparation for *IEEE Trans. Aerospace & Electronic Systems*.
6. P.S. Tan, J. Jakabosky, J.M. Stiles, and S.D. Blunt, "Higher-Order Polyphase-Coded FM Radar Waveforms," in preparation for *IET Radar, Sonar & Navigation*.

7. J. Jakabosky, S.D. Blunt, and B. Himed, “On ‘Over-Coded’ Structures for Radar Waveforms,” in preparation for *IEEE Trans. Aerospace & Electronic Systems*.
8. D. Henke, P. McCormick, S.D. Blunt, and T. Higgins, “Robust Optimal & Adaptive Pulse Compression for FM Radar Waveforms,” in preparation for *IET Radar, Sonar & Navigation*.

Conference

1. H. Griffiths, S. Blunt, L. Cohen, L. Savy, “Challenge Problems in Spectrum Engineering and Waveform Diversity,” *IEEE Radar Conference*, Ottawa, Canada, 29 Apr. - 3 May 2013. (INVITED)
2. S.A. Seguin, J. Jakabosky, B.D. Cordill, and S. Blunt, “Phased Array Antenna Model-in-the-Loop Radar Waveform Optimization,” *IEEE Intl. Conf. on Microwaves, Communications, Antennas and Electronic Systems*, Tel Aviv, Israel, 21-23 Oct. 2013. (INVITED)
3. L. Ryan, J. Jakabosky, S.D. Blunt, C. Allen, and L. Cohen, "Optimizing Polyphase-Coded FM Waveforms within a LINC Transmit Architecture," *IEEE Radar Conference*, Cincinnati, OH, 19-23 May 2014.
4. B.D. Cordill, S.A. Seguin, and S.D. Blunt, “Mutual Coupling Calibration using the Reiterative Superresolution (RISR) Algorithm,” *IEEE Radar Conference*, Cincinnati, OH, 19-23 May 2014, pp. 1278-1282.
5. J. Jakabosky, S.D. Blunt, and B. Himed, “Optimization of “Over-coded” Radar Waveforms,” *IEEE Radar Conference*, Cincinnati, OH, 19-23 May 2014, pp. 1460-1465.
6. S.D. Blunt, P. McCormick, T. Higgins, and M. Rangaswamy, “Spatially-Modulated Radar Waveforms Inspired by Fixational Eye Movement,” *IEEE Radar Conference*, Cincinnati, OH, 19-23 May 2014, pp. 900-905.
7. S.D. Blunt, P. McCormick, T. Higgins, and M. Rangaswamy, “Adaptive Delay-Angle Processing of Physical MIMO Radar Emissions,” *NATO SET-204 Research Specialists’ Meeting on Waveform Diversity*, Berlin, Germany, 29-30 Sept. 2014.
8. S.D. Blunt, P. McCormick, J. Jakabosky, and C. Allen, “Fast-Time Polarization Modulation using PCFM Radar Waveforms,” *NATO SET-204 Research Specialists’ Meeting on Waveform Diversity*, Berlin, Germany, 29-30 Sept. 2014.
9. P. McCormick, J. Jakabosky, S.D. Blunt, C. Allen, and B. Himed, “Joint Polarization/Waveform Design and Adaptive Receive Processing,” *IEEE International Radar Conference*, Washington, DC, 11-15 May 2015. (INVITED)
10. D. Henke, P. McCormick, S.D. Blunt, and T. Higgins, “Practical Aspects of Optimal Mismatch Filtering and Adaptive Pulse Compression for FM Waveforms,” *IEEE International Radar Conference*, Washington, DC, 11-15 May 2015.

11. P.S. Tan, J. Jakabosky, J.M. Stiles, and S.D. Blunt, “On Higher-Order Representations of Polyphase-Coded FM Radar Waveforms,” *IEEE International Radar Conference*, Washington, DC, 11-15 May 2015.
12. P. McCormick and S.D. Blunt, “Fast-Time 2-D Spatial Modulation of Physical Radar Emissions,” *International Radar Symposium*, Dresden, Germany, 24-26 June 2015. (INVITED)
13. J. Jakabosky, S.D. Blunt, and A. Martone, “Incorporating Spectral Gaps into Nonrecurrent FMCW Radar Leveraging Cognitive Spectrum Sensing,” submitted to *IEEE Intl. Workshop on Computational Advances in Multi-Sensor Adaptive Processing*, Cancun, Mexico, 13-16 Dec. 2015. (INVITED)

Theses/Dissertations

1. L.S. Ryan, "Polyphase-Coded FM Waveform Optimization within a LINC Transmit Architecture," Master's Thesis, University of Kansas, January 2014.
2. B. Cordill, "Radar System Enhancement Through High Fidelity Electromagnetic Modeling," PhD Dissertation, University of Kansas, April 2014.
3. J. Metcalf, "Signal Processing for Non-Gaussian Statistics: Clutter Distribution Identification and Adaptive Threshold Estimation," PhD Dissertation, University of Kansas, March 2015.
4. D. Henke, "Robust Optimal and Adaptive Radar Pulse Compression of FM Waveforms," Master's Thesis, University of Kansas, expected Fall 2015.
5. P. McCormick, "Robust Optimal and Adaptive Radar Pulse Compression of FM Waveforms," Master's Thesis, University of Kansas, expected Fall 2015.
6. J. Jakabosky, "On the Optimization of Physical Radar Emissions," PhD Dissertation, University of Kansas, expected Fall 2016.

Invited Presentations

1. "Design of Physical Radar Emissions for Waveform-Diverse Modalities," *AFRL Cognitive RF Workshop*, Albuquerque, NM, 26-27 Sept. 2012.
2. "The Links between Cognitive Sensing and Optimization of Physical Emissions" *Cognitive Radar Working Group* (AFOSR, AFRL, and University Consortia), Dayton, OH, 31 Jan. 2013.
3. S.A. Seguin, J. Jakabosky, B.D. Cordill, and S. Blunt, "Phased Array Antenna Model-in-the-Loop Radar Waveform Optimization," *IEEE Intl. Conf. on Microwaves, Communications, Antennas and Electronic Systems*, Tel Aviv, Israel, 21-23 Oct. 2013.
4. P. McCormick, J. Jakabosky, S.D. Blunt, C. Allen, and B. Himed, "Joint Polarization/Waveform Design and Adaptive Receive Processing," *IEEE International Radar Conference*, Washington, DC, 11-15 May 2015.
5. P. McCormick and S.D. Blunt, "Fast-Time 2-D Spatial Modulation of Physical Radar Emissions," *International Radar Symposium*, Dresden, Germany, 24-26 June 2015.
6. J. Jakabosky, S.D. Blunt, and A. Martone, "Incorporating Spectral Gaps into Nonrecurrent FMCW Radar Leveraging Cognitive Spectrum Sensing," submitted to *IEEE Intl. Workshop on Computational Advances in Multi-Sensor Adaptive Processing*, Cancun, Mexico, 13-16 Dec. 2015.

Research Collaborations

The following individuals have participated in the project through collaborative research efforts.

Prof. Chris Allen (University of Kansas)
Mr. Lawrence Cohen (NRL Radar Division)
Mr. Matthew Cook (Garmin)
Prof. Hugh Griffiths (University College London)
Dr. Thomas Higgins (NRL Radar Division)
Dr. Braham Himed (AFRL Sensors Directorate)
Dr. Anthony Martone (ARL Sensors & Electron Devices Directorate)
Dr. Eric Mokole (NRL Radar Division – retired)
Dr. Muralidhar Rangaswamy (AFRL Sensors Directorate)
Mr. Laurent Savy (ONERA, France)
Prof. Sarah Seguin (University of Kansas)
Prof. James Stiles (University of Kansas)

Student Research Collaborations

Graduate Students
Mr. Lane Ryan – completed MS EE in January 2014 (now at Honeywell FM&T)
Dr. Brian Cordill – completed PhD EE in April 2014 (now at Boeing Satellite Sys.)
Dr. Justin Metcalf – completed PhD EE in May 2015 (now at AFRL Sensors Dir.)
Mr. Cenk Sahin – expected PhD EE in Fall 2015
Mr. Dakota Henke – expected MS EE in Fall 2015
Ms. Audrey Seybert – expected MS EE in Spring 2016
Mr. John Jakabosky – expected PhD EE in Fall 2016
Mr. Peng Seng Tan – expected PhD EE in Fall 2016
Mr. Patrick McCormick – expected MS EE in Fall 2015 & PhD EE in Fall 2017

References

[1] H. Griffiths, S. Blunt, L. Cohen, L. Savy, "Challenge problems in spectrum engineering and waveform diversity," *IEEE Radar Conference*, Ottawa, Canada, 29 Apr. - 3 May 2013.

[2] M. Wicks, E. Mokole, S.D. Blunt, V. Amuso, and R. Schneible, eds., *Principles of Waveform Diversity & Design*, SciTech Publishing, 2010.

[3] S. Blunt, M. Cook, E. Perrins, and J. de Graaf, "CPM-based radar waveforms for efficiently bandlimiting a transmitted spectrum," *IEEE Radar Conf*., Pasadena, CA, May 2009.

[4] S.D. Blunt, M. Cook, J. Jakabosky, J. de Graaf, and E. Perrins, "Polyphase-coded FM (PCFM) radar waveforms, part I: implementation," *IEEE Trans. Aerospace & Electronic Systems*, vol. 50, no. 3, pp. 2218-2229, July 2014.

[5] S.D. Blunt, J. Jakabosky, M. Cook, J. Stiles, S. Seguin, and E.L. Mokole, "Polyphase-coded FM (PCFM) radar waveforms, part II: optimization," *IEEE Trans. Aerospace & Electronic Systems*, vol. 50, no. 3, pp. 2230-2241, July 2014.

[6] J. Jakabosky, P. Anglin, M.R. Cook, S.D. Blunt, and J. Stiles, "Non-linear FM waveform design using marginal Fisher's information within the CPM framework," *IEEE Radar Conf.,* pp. 513-518, Kansas City, MO, May 2011.

[7] J. Jakabosky, S.D. Blunt, M.R. Cook, J. Stiles, and S.A. Seguin, "Transmitter-in-the-loop optimization of physical radar emissions," *IEEE Radar Conf.*, pp. 874-879, Atlanta, GA, May 2012.

[8] T. Collins and P. Atkins, "Nonlinear frequency modulation chirps for active sonar," *IEE Proc. Radar, Sonar & Navigation*, vol. 146, no. 6, pp. 312-316, Dec. 1999.

[9] E. Fowle, "The design of FM pulse compression signals," *IEEE Trans. Information Theory*, vol. 10, no. 1, pp. 61-67, Jan. 1964.

[10] C.E. Cook, "A class of nonlinear FM pulse compression signals," *Proceedings of the IEEE*, vol. 52, no. 11, pp. 1369-1371, Nov. 1964.

[11] R. De Buda, "Stationary phase approximations of FM spectra," *IEEE Trans. Information Theory*, vol. 12, no. 3, pp. 305-311, July 1966.

[12] J.A. Johnston and A.C. Fairhead, "Waveform design and Doppler sensitivity analysis for nonlinear FM chirp pulses," *IEE Proc. F – Communications, Radar & Signal Processing*, vol. 133, no. 2, pp. 163-175, Apr. 1986.

[13] N. Levanon and E. Mozeson, *Radar Signals*, John Wiley & Sons, Inc., Hoboken, NJ, 2004.

[14] M. Vespe, G. Jones, and C.J. Baker, "Lesson for radar: waveform diversity in echolocating mammals," *IEEE Signal Processing Magazine*, vol. 26, no. 1, pp. 65-75, Jan. 2009.

[15] J. Jakabosky, S.D. Blunt, and B. Himed, “Waveform design and receive processing for nonrecurrent nonlinear FMCW radar,” *IEEE International Radar Conference*, Washington, DC, 11-15 May 2015.

[16] J. Jakabosky, S.D. Blunt, and A. Martone, “Incorporating spectral gaps into nonrecurrent FMCW radar leveraging cognitive spectrum sensing,” submitted to *IEEE Intl. Workshop on Computational Advances in Multi-Sensor Adaptive Processing*, Cancun, Mexico, 13-16 Dec. 2015.

[17] S.D. Blunt, P. McCormick, T. Higgins, and M. Rangaswamy, “Spatially-modulated radar waveforms inspired by fixational eye movement,” *IEEE Radar Conference*, Cincinnati, OH, 19-23 May 2014, pp. 900-905.

[18] S.D. Blunt, P. McCormick, T. Higgins, and M. Rangaswamy, "Physical emission of spatially-modulated radar," *IET Radar, Sonar & Navigation*, vol. 8, no. 12, pp. 1234-1246, Dec. 2014.

[19] P. Antonik, M.C. Wicks, H.D. Griffiths, and C. J. Baker, “Range-dependent beamforming using element level waveform diversity,” *International Waveform Diversity and Design Conference*, Lihue, HI, Jan. 2006.

[20] P. Baizert, T.B. Hale, M.A. Temple, and M.C. Wicks, “Forward-looking radar GMTI benefits using a linear frequency diverse array,” *IEE Electronics Letters*, vol. 42, no. 22, pp. 1311-1312, Oct. 2006.

[21] M. Secmen, S. Demir, A. Hizal, and T. Eker, “Frequency diverse array antenna with periodic time modulated pattern in range and angle,” *IEEE Radar Conference*, Waltham, MA, Apr. 2007, pp. 427-430.

[22] T. Higgins and S.D. Blunt, “Analysis of range-angle coupled beamforming with frequency-diverse chirps,” *International Waveform Diversity & Design Conference*, Orlando, FL, Feb. 2009, pp. 140-144.

[23] P.F. Sammartino, C.J. Baker, and H.D. Griffiths, “Frequency diverse MIMO techniques for radar,” *IEEE Trans. Aerospace & Electronic Systems*, vol. 49, no. 1, pp. 201-222, Jan. 2013.

[24] B. Cordill, J. Metcalf, S.A. Seguin, D. Chatterjee, and S.D. Blunt, “The Impact of Mutual Coupling on MIMO Radar Emissions,” *IEEE International Conference on Electromagnetics in Advanced Applications*, Turino, Italy, 12-17 Sept. 2011.

[25] G. Babur, P.J. Aubry, and F. Le Chevalier, “Antenna coupling effects for space-time radar waveforms: analysis and calibration,” *IEEE Trans. Antennas & Propagation*, vol. 62, no. 5, pp. 2572–2586, May 2014.

[26] G. Frazer, Y. Abramovich, and B. Johnson, ”Spatially waveform diverse radar: perspectives for high frequency OTHR”, *IEEE Radar Conference*, pp. Boston, MA, Apr. 2007, pp. 385–390.

[27] F. Daum and J. Huang, “MIMO radar: snake oil or good idea?” *IEEE Aerospace and Electronic Systems Magazine*, vol. 24, no. 5, pp. 8-12, May 2009.

[28] P. McCormick and S.D. Blunt, “Fast-time 2-D spatial modulation of physical radar emissions,” *International Radar Symposium*, Dresden, Germany, 24-26 June 2015.

[29] M. Rolfs, “Microsaccades: small steps on a long way,” *Vision Research*, vol. 49, pp. 2415-2441, 2009.

[30] E. Ahissar and A. Arieli, “Seeing via miniature eye movements: a dynamic hypothesis for vision,” *Frontiers in Computational Neuroscience*, vol. 6, no. 89, Nov. 2012.

[31] J. Cui, M. Wilke, N.K. Logothetis, D.A. Leopold, and H. Liang, “Visibility states modulate microsaccade rate and direction,” *Vision Research*, vol. 49, pp. 228-236, 2009.

[32] V.N. Bringi and V. Chandrasekar, *Polarimetric Doppler Weather Radar: Principles and Applications*, Cambridge, U.K.: Cambridge Univ. Press, 2001.

[33] J.J. van Zyl and Y. Kim, *Synthetic Aperture Radar Polarimetry*, John Wiley & Sons, Inc., Nov. 2011.

[34] D. Giuli, L. Facheris, M. Fossi, and A. Rossettini, “Simultaneous scattering matrix measurement through signal coding,” *IEEE International Radar Conference*, Arlington, VA, May 1990.

[35] D. Giuli, M. Fossi, and L. Facheris, "Radar target scattering matrix measurement through orthogonal signals," *IEE Proceedings F: Radar and Signal Processing*, vol. 140, no. 4, pp. 233-242, Aug. 1993.

[36] L. Ryan, J. Jakabosky, S.D. Blunt, C. Allen, and L. Cohen, "Optimizing polyphase-coded FM waveforms within a LINC transmit architecture," *IEEE Radar Conference*, Cincinnati, OH, 19-23 May 2014.

[37] P. McCormick, J. Jakabosky, S.D. Blunt, C. Allen, and B. Himed, “Joint polarization/waveform design and adaptive receive processing,” *IEEE International Radar Conference*, Washington, DC, 11-15 May 2015.

[38] P. McCormick, J. Jakabosky, S.D. Blunt, C. Allen, and B. Himed, “Adaptive polarimetric radar receive processing and fast-time polarization modulation,” in preparation for *IEEE Trans. Aerospace & Electronic Systems*.

[39] J. Jakabosky, S.D. Blunt, and B. Himed, “Optimization of “over-coded” radar waveforms,” *IEEE Radar Conference*, Cincinnati, OH, 19-23 May 2014, pp. 1460-1465.

[40] J. Jakabosky, S.D. Blunt, and B. Himed, “On ‘over-coded’ structures for radar waveforms,” in preparation for *IEEE Trans. Aerospace & Electronic Systems*.

[41] J. Jakabosky, S.D. Blunt, and T. Higgins, “Ultra-low sidelobe waveform design via spectral shaping and LINC transmit architecture,” *IEEE International Radar Conf*erence, Washington, DC, 11-15 May 2015.

[42] P.S. Tan, J. Jakabosky, J.M. Stiles, and S.D. Blunt, “On higher-order representations of polyphase-coded FM radar waveforms,” *IEEE International Radar Conference*, Washington, DC, 11-15 May 2015.

[43] P.S. Tan, J. Jakabosky, J.M. Stiles, and S.D. Blunt, “Higher-order polyphase-coded FM radar waveforms,” in preparation for *IET Radar, Sonar & Navigation*.

[44] M.H. Ackroyd and F. Ghani, “Optimum mismatch filters for sidelobe suppression,” *IEEE Trans. AES*, vol. AES-9, no. 2, pp. 214-218, Mar. 1973.

[45] S.D. Blunt and K. Gerlach, “Adaptive pulse compression via MMSE estimation,” *IEEE Trans. Aerospace & Electronic Systems*, vol. 42, no. 2, pp. 572-584, April 2006.

[46] D. Henke, P. McCormick, S.D. Blunt, and T. Higgins, “Practical aspects of optimal mismatch filtering and adaptive pulse compression for FM waveforms,” *IEEE International Radar Conference*, Washington, DC, 11-15 May 2015.

[47] D. Henke, P. McCormick, S.D. Blunt, and T. Higgins, “Robust optimal & adaptive pulse compression for FM radar waveforms,” in preparation for *IET Radar, Sonar & Navigation*

[48] T. Higgins, S.D. Blunt, and K. Gerlach, “Gain-constrained adaptive pulse compression via an MVDR framework,” *IEEE Radar Conference*, Pasadena, CA, 4-8 May 2009.

[49] S.D. Blunt and T. Higgins, “Dimensionality reduction techniques for efficient adaptive radar pulse compression,” *IEEE Trans. Aerospace & Electronic Systems*, vol. 46, no. 1, pp. 349-362, Jan. 2010.

[50] S.D. Blunt, K. Gerlach, and T. Higgins, “Aspects of radar range super-resolution,” *IEEE Radar Conference*, Waltham, MA, 17-20 April 2007.

[51] S.D. Blunt, T. Chan, and K. Gerlach, “A new framework for direction-of-arrival estimation,” *IEEE Sensor Array and Multichannel Processing Workshop*, Darmstadt, Germany, 21-23 July 2008.

[52] S.D. Blunt, T. Chan, and K. Gerlach, “Robust DOA estimation: the re-iterative super-resolution (RISR) algorithm,” *IEEE Trans. Aerospace & Electronic Systems*, vol. 47, no. 1, pp. 332-346, Jan. 2011.

[53] T. Higgins, S.D. Blunt, and A.K. Shackelford, “Space-range adaptive processing for waveform-diverse radar imaging,” *IEEE International Radar Conference*, Washington, DC, 10-14 May 2010.

[54] P. McCormick, T. Higgins, S.D. Blunt, and M. Rangaswamy, "Adaptive receive processing of spatially-modulated physical radar emissions," accepted to *IEEE Journal of Special Topics in Signal Processing*.

[55] S.D. Blunt and P. Yatham, “Waveform design for radar-embedded communications,” *International Waveform Diversity & Design Conference*, Pisa, Italy, 4-8 June 2007.

[56] S.D. Blunt, P. Yatham, and J. Stiles, “Intra-pulse radar-embedded communications,” *IEEE Trans. Aerospace & Electronic Systems*, vol. 46, no. 3, pp. 1185-1200, July 2010.

[57] S.D. Blunt, J.G. Metcalf, C.R. Biggs, and E. Perrins, “Performance characteristics and metrics for intra-pulse radar-embedded communication,” *IEEE Journal on Selected Areas in Communications*, vol. 29, no. 10, pp. 2057-2066, Dec. 2011

[58] J.G. Metcalf, C. Sahin, S.D. Blunt, and M. Rangaswamy, "Analysis of symbol design strategies for intrapulse radar-embedded communications," accepted to *IEEE Trans. Aerospace & Electronic Systems*.

1.

1. Report Type

Final Report

Primary Contact E-mail

Contact email if there is a problem with the report.

sdblunt@ittc.ku.edu

Primary Contact Phone Number

Contact phone number if there is a problem with the report

703-975-1921

Organization / Institution name

University of Kansas

Grant/Contract Title

The full title of the funded effort.

Multidimensional Signal Processing for Sensing & Communications

Grant/Contract Number

AFOSR assigned control number. It must begin with "FA9550" or "F49620" or "FA2386".

FA9550-12-1-0220

Principal Investigator Name

The full name of the principal investigator on the grant or contract.

Shannon D. Blunt

Program Manager

The AFOSR Program Manager currently assigned to the award

Dr. Arje Nachman

Reporting Period Start Date

06/01/2012

Reporting Period End Date

05/31/2015

Abstract

The objective of this effort was to enhance sensitivity and develop new multi-mode formulations for radar and communications in the presence of interference, which may be coupled across the dimensions of space, slow-time, fast-time, and polarization according to the operating mode. In particular, the effort focused on waveform-diverse emission schemes such as various physically realizable forms of MIMO radar and polarization-diverse radar, adaptive receive processing for these waveform-diverse modes, and intra-pulse radar-embedded communications.

Leveraging the notion of STAP used for clutter cancellation in airborne/space radar, the multiplicative increase in degrees of freedom afforded by multidimensional coupling enables expansion to other dimensions as well. Performing this coupling on transmit also has the potential to improve receive detection/estimation performance via the resulting increased diversity of the transmit signal. This effort addressed the mathematical modeling and optimization of different multidimensional structures for the realization of new physical radar emissions which, when possible based on available test equipment, were also evaluated experimentally.

New adaptive receiver processing schemes were also likewise developed for these multidimensional emission structures which were also evaluated experimentally based on the availability of measurements.

Finally, this effort continued the theoretical development of a scheme for waveform-diverse embedding of

low probability of intercept communication symbols into radar clutter, along with associated symbol detection/decision processing, that was the focus of a previous AFOSR YIP award. It is expected that, upon transition, these waveform-diverse schemes will serve as enabling technology to support long-term Air Force initiatives to address an ever more congested and contested RF spectrum.

Distribution Statement

This is block 12 on the SF298 form.

Distribution A - Approved for Public Release

Explanation for Distribution Statement

If this is not approved for public release, please provide a short explanation. E.g., contains proprietary information.

SF298 Form

Please attach your SF298 form. A blank SF298 can be found here. Please do not password protect or secure the PDF The maximum file size for an SF298 is 50MB.

SF0298c.pdf

Upload the Report Document. File must be a PDF. Please do not password protect or secure the PDF . The maximum file size for the Report Document is 50MB.

Blunt AFOSR Final Report - 2015.pdf

Upload a Report Document, if any. The maximum file size for the Report Document is 50MB.

Archival Publications (published) during reporting period:

S.D. Blunt, J. Jakabosky, M. Cook, J. Stiles, S. Seguin, and E.L. Mokole, "Polyphase-Coded FM (PCFM) Radar Waveforms, Part II: Optimization," IEEE Trans. Aerospace & Electronic Systems, vol. 50, no. 3, pp. 2230-2241, July 2014.

S.D. Blunt, P. McCormick, T. Higgins, and M. Rangaswamy, "Physical Emission of Spatially-Modulated Radar," IET Radar, Sonar & Navigation, vol. 8, no. 12, pp. 1234-1246, Dec. 2014.

P. McCormick, T. Higgins, S.D. Blunt, and M. Rangaswamy, "Adaptive Receive Processing of Spatially-Modulated Physical Radar Emissions," accepted to IEEE Journal of Special Topics in Signal Processing. (special issue on Advanced Signal Processing Techniques for Radar Applications)

J.G. Metcalf, C. Sahin, S.D. Blunt, and M. Rangaswamy, "Analysis of Symbol Design Strategies for Intrapulse Radar-Embedded Communications," accepted to IEEE Trans. Aerospace & Electronic Systems.

H. Griffiths, S. Blunt, L. Cohen, L. Savy, “Challenge Problems in Spectrum Engineering and Waveform Diversity,” IEEE Radar Conference, Ottawa, Canada, 29 Apr. - 3 May 2013.

S.A. Seguin, J. Jakabosky, B.D. Cordill, and S. Blunt, “Phased Array Antenna Model-in-the-Loop Radar Waveform Optimization,” IEEE Intl. Conf. on Microwaves, Communications, Antennas and Electronic Systems, Tel Aviv, Israel, 21-23 Oct. 2013.

L. Ryan, J. Jakabosky, S.D. Blunt, C. Allen, and L. Cohen, "Optimizing Polyphase-Coded FM Waveforms within a LINC Transmit Architecture," IEEE Radar Conference, Cincinnati, OH, 19-23 May 2014.

B.D. Cordill, S.A. Seguin, and S.D. Blunt, “Mutual Coupling Calibration using the Reiterative Superresolution (RISR) Algorithm,” IEEE Radar Conference, Cincinnati, OH, 19-23 May 2014, pp. 1278-1282.

J. Jakabosky, S.D. Blunt, and B. Himed, “Optimization of “Over-coded” Radar Waveforms,” IEEE Radar Conference, Cincinnati, OH, 19-23 May 2014, pp. 1460-1465.

S.D. Blunt, P. McCormick, T. Higgins, and M. Rangaswamy, “Spatially-Modulated Radar Waveforms

Inspired by Fixational Eye Movement," IEEE Radar Conference, Cincinnati, OH, 19-23 May 2014, pp. 900-905.

S.D. Blunt, P. McCormick, T. Higgins, and M. Rangaswamy, "Adaptive Delay-Angle Processing of Physical MIMO Radar Emissions," NATO SET-204 Research Specialists' Meeting on Waveform Diversity, Berlin, Germany, 29-30 Sept. 2014.

S.D. Blunt, P. McCormick, J. Jakabosky, and C. Allen, "Fast-Time Polarization Modulation using PCFM Radar Waveforms," NATO SET-204 Research Specialists' Meeting on Waveform Diversity, Berlin, Germany, 29-30 Sept. 2014.

P. McCormick, J. Jakabosky, S.D. Blunt, C. Allen, and B. Himed, "Joint Polarization/Waveform Design and Adaptive Receive Processing," IEEE International Radar Conference, Washington, DC, 11-15 May 2015.

D. Henke, P. McCormick, S.D. Blunt, and T. Higgins, "Practical Aspects of Optimal Mismatch Filtering and Adaptive Pulse Compression for FM Waveforms," IEEE International Radar Conference, Washington, DC, 11-15 May 2015.

P.S. Tan, J. Jakabosky, J.M. Stiles, and S.D. Blunt, "On Higher-Order Representations of Polyphase-Coded FM Radar Waveforms," IEEE International Radar Conference, Washington, DC, 11-15 May 2015.

P. McCormick and S.D. Blunt, "Fast-Time 2-D Spatial Modulation of Physical Radar Emissions," International Radar Symposium, Dresden, Germany, 24-26 June 2015.

Changes in research objectives (if any):

None.

Change in AFOSR Program Manager, if any:

Original PM was Dr. Jon Sjogren. Current PM is Dr. Arje Nachman.

Extensions granted or milestones slipped, if any:

None.

AFOSR LRIR Number

LRIR Title

Reporting Period

Laboratory Task Manager

Program Officer

Research Objectives

Technical Summary

Funding Summary by Cost Category (by FY, $K)

	Starting FY	FY+1	FY+2
Salary			
Equipment/Facilities			
Supplies			
Total			

Report Document

Report Document - Text Analysis

Report Document - Text Analysis

Appendix Documents

2. Thank You

E-mail user

Jul 28, 2015 15:00:06 Success: Email Sent to: sdblunt@ittc.ku.edu